Front. Med. 2024, 18(3): 516–537
https://doi.org/10.1007/s11684-023-1024-8

RESEARCH ARTICLE

A distinct “repair” role of regulatory T cells in fracture healing

Tingting Wu[1,2,*], Lulu Wang[1,2,*], Chen Jian[1,2], Zhenhe Zhang[3], Ruiyin Zeng[3], Bobin Mi[3], Guohui Liu[3], Yu Zhang[1,2], Chen Shi (✉)[1,2]

[1]Department of Pharmacy, Union Hospital, Tongji Medical College, Huazhong University of Science and Technology, Wuhan 430022, China; [2]Hubei Province Clinical Research Center for Precision Medicine for Critical Illness, Wuhan 430022, China; [3]Department of Orthopedics, Union Hospital, Tongji Medical College, Huazhong University of Science and Technology, Wuhan 430022, China

Abstract **Regulatory T cells (Tregs) suppress immune responses and inflammation. Here, we described the distinct nonimmunological role of Tregs in fracture healing. The recruitment from the circulation pool, peripheral induction, and local expansion rapidly enriched Tregs in the injured bone. The Tregs in the injured bone displayed superiority in direct osteogenesis over Tregs from lymphoid organs. Punctual depletion of Tregs compromised the fracture healing process, which leads to increased bone nonunion. In addition, bone callus Tregs showed unique T-cell receptor repertoires. Amphiregulin was the most overexpressed protein in bone callus Tregs, and it can directly facilitate the proliferation and differentiation of osteogenic precursor cells by activation of phosphatidylinositol 3-kinase/protein kinase B signaling pathways. The results of loss- and gain-function studies further evidenced that amphiregulin can reverse the compromised healing caused by Treg dysfunction. Tregs also enriched in patient bone callus and amphiregulin can promote the osteogenesis of human pre-osteoblastic cells. Our findings indicate the distinct and nonredundant role of Tregs in fracture healing, which will provide a new therapeutic target and strategy in the clinical treatment of fractures.**

Keywords regulatory T cells; fracture healing; amphiregulin; non-union; osteogenesis

Introduction

Regulatory T cells (Tregs), particularly the subset expressing X-chromosome-encoded transcription factor Foxp3, are crucial in maintain immune homeostasis, including the innate and adaptive immune networks, prevention of autoimmune diseases, and regulation of inflammatory processes [1,2]. Tregs mainly populate in lymphoid organs, and a small portion resides in nonlymphoid tissues. These cells can be classically divided into three populations: thymus-derived (tTregs), periphery-induced (pTregs), and induced Tregs (iTregs) [3]. tTregs are the dominant form of Tregs, and they are mainly responsible for the control of Treg development in the thymus and maintaining most Treg activities and immune regulatory functions [4,5]. In addition, tTregs regulate the immune responses of various cell types with several specific but partially overlapping mechanisms. iTregs develop from naïve T cells after stimulation by cytokines, such as tumor growth factor β (TGF-β) and interleukin (IL)-2 [6]. Meanwhile, pTregs, which are located in different tissues, display considerable heterogeneity, including the expression of various phenotypes, chemokine receptors or effector molecules, T cell receptors (TCRs), and mechanism of functions [7]. pTregs have been highlighted to have nontraditional functions that modulate extraimmunological processes. The initially characterized pTregs were the Tregs in visceral adipose tissue (VAT) described by Mathis’ group [8]. They observed that a population of Tregs with a unique phenotype was highly enriched in the VAT of lean, aged male mice. Moreover, Treg accumulation was primarily driven by peroxisome proliferator-activated receptor-γ, which enabled the mice to function in glucose metabolism and thereby alleviate insulin resistance [9]. They also discovered another tissue-resident population of Tregs that infiltrated injured skeletal muscle and acted with muscle satellite cells and improved muscle repair [10]. Inspired by this kind of specific “repair” feature, the Treg functions in other tissues were studied by various researchers. Notably, Tregs promote the repair of infectious lung injury [11], myocardial infarction [12],

Received April 17, 2023; accepted July 20, 2023
Correspondence: Chen Shi, whxhchen@163.com

*These authors contributed equally to this work.

neovascular retinopathies [13], and skin [14]. However, the role of Tregs in bone, especially during fracture, remains largely elusive.

Bone fracture is a common clinical injury that causes serious life and economic burdens to patients. The individual lifetime prevalence of fracture can reach as high as 50% [15]. Although most bone injuries can heal normally, 5%–10% of patients still suffer from delayed healing or nonunion [16,17]. Fracture healing must be promoted to improve clinical outcomes in trauma medicine. In 1972, Horton *et al*. [18] initially discovered that the activation of leukocytes in peripheral blood promotes osteoclastogenesis, which indicates a regulatory relationship between the immune system and bones. In 2000, Arron *et al*. [19] formally proposed the concept of bone immunology. In 2018, Baht *et al*. [15] discussed the functional roles of immune cells in fracture healing and divided the process into four phases: inflammatory, cartilaginous callus formation, bony callus formation, and remodeling phases. Various immune cells intervene in each stage and participate in bone remodeling. Therefore, the immune system plays a crucial regulatory role in bone healing. Recent studies have reported the importance of Tregs in osteoimmunity [20,21]. Typically, Tregs can reduce the inflammatory response after bone injury through their inherent immunosuppressive properties. Cytotoxic T lymphocyte-associated antigen-4 (CTLA-4) expressed on Treg surface can make contact with CD80/CD86 on dendritic cells, which consequently inhibits the activation of effector T cells and reduces proinflammatory cytokine secretion and antibody production [20]. Tregs also secrete immunosuppressive cytokines, such as TGF-β, IL-10, and IL-4, to regulate osteoclastogenesis [21]. Given that Tregs display extraimmunological roles in other tissue repair, Tregs are perhaps also endowed with unique bone functions. However, whether and how Tregs participate in the bone healing process remain unclear.

In this study, we sought to answer these questions and identify the nonimmunological role of Tregs in fracture healing. First, the proportion of Tregs in different tissues was analyzed to clarify their accumulation in injured bone. In addition, circulating block experiments, thymus marker detection, and cell expansion assays were performed to study the source of enriched Tregs. Then, we sorted the Tregs in bone callus and lymphoid organs via flow cytometry (FCM) and incubated them with bone marrow mesenchymal stem cells (BMSCs, osteogenic precursor cells) to investigate their *in vitro* osteogenic capacity. The *in vivo* role of bone callus Tregs in fracture healing was studied via loss-of-function experiments. Single-cell sequencing was carried out to analyze the phenotypes of Tregs in injured bone and lymphoid organs. Differential genes were compared, and amphiregulin was identified as a possible molecule in bone callus Tregs that modulate the healing process. Then, *in vitro* BMSC proliferation and osteogenic differentiation assays and *in vivo* loss-and gain-of function experiments were performed to evaluate the activity of amphiregulin in improving fracture healing. Western blotting assay was conducted to evaluate the underlying mechanism of amphiregulin-mediated osteogenic precursor cell differentiation. In addition, the phosphatidyl inositide 3-kinases/protein kinase B (PI3K/AKT) signaling pathway was proven to be involved in this process. Lastly, we investigated the proportion of Tregs that remained after human fracture and the function of amphiregulin in human preosteoblastic cells (umbilical cord mesenchymal stem cells, hUC-MSCs). This study can provide insights into the development of new therapeutic targets for clinical fracture treatment.

Materials and methods

Study approval

Male C57BL/6 mice aged 8–10 weeks were used to develop the femoral fracture model and housed under specific pathogen free conditions. All the animal experiments were approved and performed under the regulations of the Institutional Animal Care and Use Committee of Tongji Medical College, Huazhong University of Science and Technology (HUST). The mice were randomly divided into various groups before each experiment and humanely euthanized when meeting the predefined endpoints. Human bone callus and peripheral blood were obtained from fractured patients, and human umbilical cords were collected from newborns, with informed consent from all participants as approved by the Ethics Committee of Union Hospital, Tongji Medical College, HUST.

Fracture model

Male C57BL/6 mice aged 8–10 weeks were anesthetized via intraperitoneal injection of 0.1–0.2 mL/10 g 0.3% sodium pentobarbital (Merck) (0.3% w/v). The skeletal muscle was dissected to expose the femur, and a 5-gauge needle was inserted into the femoral medullary cavity from the knee joint. Then, an ophthalmic scissor was used to cut from the middle of the femur. The fracture model was completed after the skeletal muscle and epidermis were sutured layer by layer.

Treg accumulation analysis

Changes in the proportion of Tregs in various tissues were analyzed through FCM (BD Bioscience, USA). Normal mice were used as controls and referred to the day 0 group. On days 1, 3, 5, 14, and 21 after fracture, the

spleen, peripheral blood, and bone callus were collected. The lymphocytes in peripheral blood were directly purified using the mouse peripheral blood lymphocyte isolation kit (LTS1092, TBD). Single-cell suspensions of the spleen were collected through tissue trituration, and spleen lymphocytes were isolated using the mouse spleen lymphocyte isolation kit (LTS1092PK, TBD). For the isolation of lymphocytes in the bone callus, the callus was cut into ~2 mm pieces using ophthalmic scissors and incubated with 0.2% collagen I (C8140, Solarbio) and 0.2% pronase (P8360, Solarbio) at 37 °C for 40 min. Then, the single-cell suspensions from the callus were collected and processed using the lymphocyte isolation kit (10831, Sigma Aldrich). The purified lymphocytes were then stained with anti-mouse CD45 (25-0451-81, eBioscience), anti-mouse CD4 (11-0041-82, eBioscience), and anti-mouse Foxp3 (12-5773-82, eBioscience) and analyzed via FCM. Five mice were polled for one set of analysis, and each experiment was repeated thrice.

Exploration of the sources of bone callus Tregs

Male C57BL/6 mice aged 8–10 weeks were used for femoral fracture construction. Spleens and bone calluses were collected on day 5 postfracture. Lymphocytes were collected as described above and stained with anti-mouse CD45, anti-mouse CD4, anti-mouse Foxp3, anti-mouse CD304 (Neuropilin-1) (145203, Biolegend), and anti-mouse/human Helios (137235, Biolegend) and detected through FCM.

The mice were injected intraperitoneally with 1 mg/kg FTY720 (SML0700, Sigma) or solvent one day before fracture and on days 1, 2, 3, and 4 after fracture. On day 5, the mice were sacrificed. Spleen and bone callus lymphocytes were collected as described above and stained with anti-mouse CD45, anti-mouse CD4, and anti-mouse Foxp3 and detected by FCM.

Treg proliferation analysis

On day 5 after fracture, the lymphocytes in the spleen and bone callus were isolated as described above. The cells were stained with anti-mouse CD45, anti-mouse CD4, anti-mouse Foxp3, and anti-mouse Ki67 (17-5689-80, Invitrogen), and the expressions of Ki67 in Treg ($CD45^+CD4^+Foxp3^+$) and conventional T cells (Tconvs) ($CD45^+CD4^+Foxp3^-$) were analyzed via FCM. The proliferation of Tregs was investigated using Click-iT Plus EdU Alexa Fluor™ 647 Flow Cytometry Assay Kit (C10634, Invitrogen). The fractured mice were injected with 1 mg 5-ethynyl-2′-deoxyuridine (EdU) on day 4 post fracture. After 24 h, the lymphocytes in the spleen and bone callus were collected, stained with anti-mouse CD45, anti-mouse CD4, and anti-mouse Foxp3 and detected through FCM. Each experiment was repeated thrice.

FCM sorting of Tregs

Male C57BL/6 mice aged 8–10 weeks were used for the femoral fracture model. The mice were sacrificed on day 5. The spleens, nondraining lymph nodes, and bone calluses were separated for analysis. Tregs from spleen and bone callus were obtained as described above. The lymph nodes were grinded into cell suspension, and the lymphocytes were collected after filtration and centrifugation. Non-$CD4^+$ cells were depleted through magnetic cell separation (MACS) using the $CD4^+CD25^+$ Regulatory T cell Isolation Kit (130-091-041, Miltenyi Biotec). Then, the single-cell suspension was incubated with anti-mouse CD45 (553075, BD Biosciences), anti-mouse CD4 (553729, BD Biosciences), and anti-mouse CD25 (553075, BD Biosciences) for 30 min at 4 °C. The dead cells were labeled using the Zombie NIR™ Fixable Viability Kit (423105, Biolegend). Fluorescence-activated cell sorting (AriaTM II, BD Biosciences, America) was used to acquire $CD4^+CD25^+$ Tregs.

Isolation and culture of BMSCs and hUC-MSCs

C57BL/6 mice were used for the separation of mouse BMSCs. The mice were soaked in 75% ethanol for 5 min before the dissection of the two hind legs using ophthalmic scissors. A 7-gauge disposable syringe was used to flush the marrow out of the bones using phosphate buffered saline (PBS). Filtered through a 70 μm screen, all cells from mouse femurs and tibias were cultured in a specialized medium (MUXMX-90011, Cyagen) at 37 °C in 5% CO_2. The medium was replaced daily. And after 7 days, spindle-shaped cells were readied for passage. Passages 2–5 BMSCs were used in the following experiments.

hUC-MSCs were acquired from the umbilical cord of a full-term fetus. The umbilical cord was washed with PBS containing 1% penicillin and 1% streptomycin to remove extravasated blood and vessels. Wharton’s Jelly tissues were peeled out, cut into approximately 1 mm^3 pieces, and incubated with 0.2% collagenase I and 0.2% pronase at 37 °C in 5% CO_2 for 30 min. Then, the tissue blocks were ground for several minutes using a disposable rubber head dropper. Finally, the remaining tissues were transferred to a culture disk provided with a specialized medium (HUXUC-90011, Cyagen). Fusiform cells crawled out of the tissue block in approximately 7 days. Passages 2–5 hUC-MSCs were used in the following experiments.

EdU assay

Cells were seeded in 96-well plates at a density of 3.0×10^4–5.0×10^4 cells per well depending on the rate of cell proliferation. After adherence, the cells were treated with

different concentrations of amphiregulin (HY-P7002, MCE; 315-36, Peprotech) for 48 h. The original medium was discarded, and the cells were washed with PBS before incubation using a medium that contained 50 μmol/L EdU (C10310-1, RiboBio) for 2 h. The following operations were carried out in accordance with the manufacturing instructions. An inverted fluorescence microscope (IX73, OLYMPUS, Japan) was used for observation and photography.

Cell Counting Kit 8 (CCK-8) assay

Cells were seeded in 96-well plates at a density of 3.0×10^3–5.0×10^3 cells per well. After adherence, the cells were treated using different concentrations of amphiregulin for 48 h and incubated for 3 h with 10 μL CCK-8 solution (BS350B, Biosharp). After incubation, the optical density (OD) of the cells at the wavelength of 450 nm was determined using a microplate reader (EnSprire, Perkin Elmer, America).

Alkaline phosphatase (ALP) staining

Cells were cultured for 14 days in 24-well plates provided with osteogenic induction culture medium (MUXMX-90021, Cyagen). ALP staining was performed on day 14 in accordance with the instructions of BCIP/NBT Alkaline Phosphatase Color Development Kit (C3206, Beyotime). The cells were fixated with 4% paraformaldehyde for 30 min at room temperature, washed thoroughly with cold PBS, and stained with ALP overnight. Then, the staining solution was discarded, and PBS was added. An inverted fluorescence microscope was used to observe and photograph the images.

Alizarin Red staining

Cells were cultured in 24-well plates, and after they grew to 80%–90% convergence, the culture medium was replaced with osteogenic induction culture medium (MUXMX-90021, Cyagen) and changed every other day. Alizarin Red staining was performed on day 21 following the instructions of Alizarin Red Solution Kit (ALIR-10001, Cyagen). The cells were gently washed twice with PBS before fixation with 4% paraformaldehyde for 30 min at room temperature. After washing off the paraformaldehyde with PBS, 1 mL Alizarin Red staining solution was added to stain the cells at room temperature for 5–10 min. Then, the staining solution was discarded, and the cells were washed thoroughly. An inverted fluorescence microscope was used to observe and photograph the images.

Western blotting assay

BMSCs were starved for 24 h before the treatment with 50 ng/mL amphiregulin with or without 10 μmol/L LY294002 (HY-10108, MCE), 0.5 μmol/L deguelin (HY-13425, MCE), and 25 μmol/L U0126 (S1901, Beyotime) for 0, 30, 60, and 90 min and 0, 3, and 7 days, separately. Proteins were extracted using radioimmunoprecipitation assay buffer (AS1004, ASPEN) containing 1% protease inhibitor (AS1006, ASPEN), and protein concentrations were measured using a BCA kit (AS1086, ASPEN). Then, sodium dodecyl sulphate-polyacrylamide gel electrophoresis and transfer were conducted. The polyvinylidene difluoride membranes were blocked with 5% nonfat milk for 1 h at room temperature. Antibodies for AKT (#4691, CTS), phosphorylated AKT (p-AKT) (#4060, CTS), Runt-related transcription factor 2 (RUNX2) (ab236639, Abcam), and bone morphogenetic protein (BMP)-2 (ab6285, Abcam) were stained overnight at 4 °C. Then, secondary antibodies were incubated for 30 min at room temperature. The results were detected via a chemiluminescence detection system.

Antibody depletion assay

A normalized closed fracture model was established using 8–10-week-old C57BL/6 mouse femur, and it received 200 μg anti-mouse CD25 monoclonal antibody (mAb; 102059, Biolegend) via intraperitoneal injection to deplete Tregs on day 3 before fracture and days 3 and 4 after fracture. The equivalent rat IgG1-λ isotype control antibody (401916, Biolegend) was administered intraperitoneally as control. The lymphocytes in the bone callus, spleen, and peripheral blood were separated, and the expression of $CD45^+CD4^+CD25^+Foxp3^+$ (anti-mouse CD25, 17-0251-82, eBioscience) was detected via FCM to investigate the Treg depletion efficiency of the antibody. X-Ray images of the mice were collected on day 1, 3, 5, 7, 14, and 21. The mice were sacrificed on day 21, and the fractured femur was dissected, stripped of muscles, and scanned using a Bruker micro-computed tomography (micro-CT) Skyscan 1276 system (Kontich, Belgium). The scan parameters were set as follows: 200 μA ray tube current; 85 kV voltage; 6.533712 μm scanning resolution; 384 ms exposure time, and 180° scanning angle. The images were reconstructed using the three-dimensional reconstruction software NRecon (v1.7.4.2, Bruker, Germany). The reconstruction parameters were adjusted to the following values: smoothing = 2; beam hardening = 8, and ring artifacts = 25%. Region-of-interests (ROIs) were analyzed using a CT Analyzer (v1.18.8.0, Bruker, Germany) to calculate the bone volume (BV), total tissue volume (TV), volume ratio (BV/TV), and bone mineral density (BMD).

Quantitative reverse transcription polymerase chain reaction (qRT-PCR) assay

StepOne™ Real-Time PCR System (Life technologies,

USA) was used to analyze the mRNA levels of osteogenesis-related proteins. On day 21, the bone callus was dissected and stored in liquid nitrogen. About 100 mg tissues were put on ice and fully grinded in 1 mL precooled TRIpure (EP013, ELK Biotechnology). A total of 250 μL chloroform was added, and the mixture was mixed for 5 min on ice. A total of 500 μL supernatant and an equal volume of precooled isopropanol were mixed and allowed to stand at −20 °C for 15 min, followed by centrifugation at 10 000× *g* for 10 min at 4 °C. After centrifugation and washing by 75% ethanol, 10 μL RNase-Free Water was added to fully dissolve the RNA. First-strand cDNA was synthesized using an M-MLV Reverse Transcriptase kit (Eq. (002), ELK Biotechnology). Then, qRT-PCR was completed on the StepOne™ Real-Time PCR instrument using QuFast SYBR Green PCR Master Mix kit (Eq. (001), ELK Biotechnology). The $^{\Delta\Delta}$CT method was used for data analysis.

Single-cell paired TCR- and RNA-sequencing

For single-cell paired TCR- and RNA-sequencing, on day 5 after fracture, 20 fractured mice were used for a single experiment. Lymphocytes from the spleen and bone callus were first purified using the lymphocyte isolation kits as described above. Then, non-$CD4^+$ cells were removed via MACS. The live $CD4^+$ T cells were sorted via FCM, followed by staining with 7-aminoactinomycin D (7AAD), anti-mouse CD45, and anti-mouse CD4 antibodies. Single-cell paired TCR- and RNA-sequencing were prepared using the 10× genomics Chromium Single-Cell Immune Profiling Solution (Genergy Biotechnology, Shanghai, China). Approximately 20 000 $CD4^+$ T cells with cell viabilities over 90% were sorted. Then, the $CD4^+$ T cells (1000 cells/μL) were encapsulated into droplets to form gel beads in emulsion (GEM). The expected mRNA barcodes were around 10 000 single cells. After the reverse-transcription procedure, the GEM was broken, and cDNA was amplified in 13 PCR cycles (98 °C_15 s, 63 °C_20 s, and 72 °C_1 min), and purified by Solid Phase Reversible Immobilization (SPRI). The second-generation sequencing library was prepared from the qualified cDNA and quantitatively inspected after fragmentation, ligation of sequencing adapters, sample index PCR, and other experimental processes. Illumina NovaSeq 6000 platform (sequencing mode PE150) was used for sequencing and FastQC software for the analysis of the quality of preprocessed data. Seurat [22,23] was used to perform clustering analysis on high-quality population cells, and cell populations were clustered using the Louvain modularity optimization algorithm. Then, the cell clusters were displayed with t-distributed stochastic neighbor embedding (tSNE), and Tregs were detected through canonical marker genes. For single-cell TCR-sequencing, the complementarity-determining region (CDR) 3 amino acid sequences of TRA or TRB were annotated using the VDJdb database for known antigenic determinants and antigenic proteins. Single-cell RNA-sequencing data were processed using the Seurat function find_all_markers [24,25].

Treatments of fractures in mice and recovery evaluation

Five groups were included in the study: sham-operated mice, Treg-depletion fracture mice with amphiregulin, Treg-depletion fracture mice with PBS, isotype control-treated mice with amphiregulin, and isotype control-treated mice with PBS. The treatment groups were injected with 1 μg recombinant murine amphiregulin (315-36, Peprotech) locally at the fracture site on days 0, 3, and 4 after surgery. Then, 5 μg amphiregulin was injected intraperitoneally on days 6 and 8 after surgery. The control groups were injected with the same volume of PBS. The X-ray images of mice were obtained on days 0, 7, 14, and 21 after fracture (In-Vivo PRO, BRUKER, Germany). On day 21, the mice were sacrificed, and their femurs were dissected with muscles stripped away. The micro-CT system (SkyScan 1176, Bruker, Germany) was used to construct a three-dimensional image of the fracture area to calculate the BMD, BV, TV, and BV/TV. The longitudinal and transverse sections of femurs were shown using CTvox software (3.3.0.0, Bruker, Germany).

Serum cytokine detection

Serum was collected through centrifugation at 3000 rpm for 10 min after the mice were sacrificed. The level of ALP was detected using an Alkaline Phosphatase Assay Kit (P0321S, Beyotime) following the manufacturer’s instruction, and the OD at the wavelength of 410 nm was determined using a microplate reader. The concentrations of bone ALP and osteocalcin (OCN) were measured via enzyme-linked immunosorbent assay (ELISA), following the instructions of Mouse Bone Alkaline Phosphatase ELISA Kit (MM-44680M2, MEIMIAN) and Mouse OC/BGP (OCN) ELISA Kit (E-EL-M0864c, Elabscience).

Histological evaluation

Femurs were harvested on day 21 after fracture, and the tissues were stripped away thoroughly. The samples were fixed in 4% paraformaldehyde for over 24 h and decalcified in ethylenediaminetetraacetic acid-2Na until the bones were easily pierced. Then, they were embedded in paraffin, cut into 5 μm-thick sections along the horizontal axis, and subjected to hematoxylin and eosin (H&E) (BP092, Biossci) and Alcian blue (AB) (BP040, Biossci) staining. Tartrate-resistant acid phosphatase

(TRAP) (BP088, Biossci) staining was completed in sections along the longitudinal axis. The sections were observed and photographed using an inverted fluorescence microscope.

Tregs analysis in fractured bone of patients

The patients who met all the following inclusion criteria were allowed to participate in the study: (1) age over 18 (including 18 years old) and under 60 years old (including 60 years old); (2) clinically diagnosed as fracture; (3) required surgery; (4) participated voluntarily and signed the informed consent in writing. These patients who met the following criteria were excluded: (1) with types of fractures that are unsuitable for surgery; (2) systemic infection or local infection of the fracture area. The peripheral blood and bone callus were collected by the surgeon. Lymphocytes in the peripheral blood and bone callus were separated and stained with anti-human CD45, anti-human CD4, and anti-human Foxp3. After incubation at 4 °C for 30 min, the cells were washed thrice with PBS and detected via FCM. For the measurement of amphiregulin expression, Tregs from bone callus and peripheral blood were sorted using FCM. qRT-PCR was conducted to determine the mRNA level of amphiregulin.

Statistical analysis

Data are represented as mean ± standard deviation (SD), processed by Prism v8 (GraphPad, USA), and analyzed by Student's *t*-test for two groups or one-way analysis of variance (ANOVA) for three or more groups. $*P < 0.05$ indicated significantly statistical difference.

Results

Treg enrichment in fractured bone

A femur fracture model was established to investigate the accumulation of Tregs after fracture. At different time points after fracture, spleen, peripheral blood, and bone callus were separated, and lymphocytes were collected for FCM analysis. Within the experimental period, no considerable change was observed in the spleen $CD4^+$ T cells (Fig. 1A–1D). For peripheral blood and bone callus, the number of $CD4^+$ T cells increased at the early phase of fracture, peaked on day 5, and gradually decreased to the baseline level with prolonged duration of fracture. These findings can be attributed to the recruitment of immune cells to injured sites in response to necrotic debris, invading pathogens, and clotting reactions during injury [26]. Although the $CD4^+$ T cells in peripheral blood and bone callus showed similar tendencies, the $CD4^+$ T cells in the latter exhibited more remarkable changes compared with those in the former (3.5-fold vs. 1.9-fold on day 5). $CD4^+$ T cells contain multiple subpopulations, which display distinct properties and functions [27]. Tregs, a typical subset of $CD4^+$ T cells, play an important role in tissue repair [28]. We then investigated the changes in Tregs after fracture by FCM. As shown in Fig. 1E–1H, Tregs in the spleen, peripheral blood, and bone callus were present in low levels before fracture (day 0), but their levels in all increased after fracture. Tregs in the spleen and peripheral blood presented similar trends with the peaks of Tregs, with values of 7.8% ± 2.7% and 13.1% ± 3.8% on day 5, respectively (Fig. 1F and 1G). Compared with those in the spleen and peripheral blood, Tregs in the bone callus exhibited more significant changes. On days 0, 1, 3, 5, 14, and 21, the proportions of Tregs reached 2.9% ± 0.8%, 4.1% ± 1.9%, 10.9% ± 1.5%, 14.8% ± 1.8%, 9.2% ± 2.5%, and 5.2% ± 0.4%, respectively (Fig. 1H). Different from the rapid decrease in the number of Tregs in the spleen and peripheral blood, Tregs in the bone callus remained at high levels on days 14 (3.2-fold vs. day 0, $P < 0.05$) and 21 (1.8-fold vs. day 0, $P < 0.05$). To directly visualize the accumulation of Tregs, we fixed and decalcified fractured bones and conducted immunofluorescence staining. As displayed in Fig. S1, the signals of red (CD4) and green fluorescence (Foxp3) were enhanced in the fractured bone compared with the normal bone. The enrichment of Tregs in the fractured bone suggests the possible role of Tregs in fracture healing.

Sources of enriched Tregs in fractured bone

The level of Tregs in bone callus increased remarkably after fracture, especially compared with those in the spleen of lymphoid organs. The accumulation of Tregs in injured sites can be derived from the circulation compartment, peripheral induction, and local cell expansion [12, 29]. We questioned whether the enriched Tregs in fractured bone may also share these sources. We have proven that the level of Tregs in peripheral blood, which can be recruited to the injured bone and be a source of bone callus Tregs, was substantially increased after fracture [7]. To clarify this concept, we treated the fractured mice with FTY720, an immunosuppressive agent that acts as a functional antagonist of S1PR1, to prevent the departure of lymphocytes from secondary lymphoid tissues to the circulating pool [30]. The percentage of $CD4^+$ T cells and Tregs dropped on day 5 post fracture, which indicates that a few Tregs in bone callus were derived from the circulating pool (Fig. 2A and 2B). To study the peripheral induction of bone callus Tregs, we measured the expressions of neuropilin-1 and Helios of Tregs on day 5 post fracture. The two markers are reported as cell markers of tTregs rather than peripherally iTregs [31–33]. Neuropilin-1 and Helios

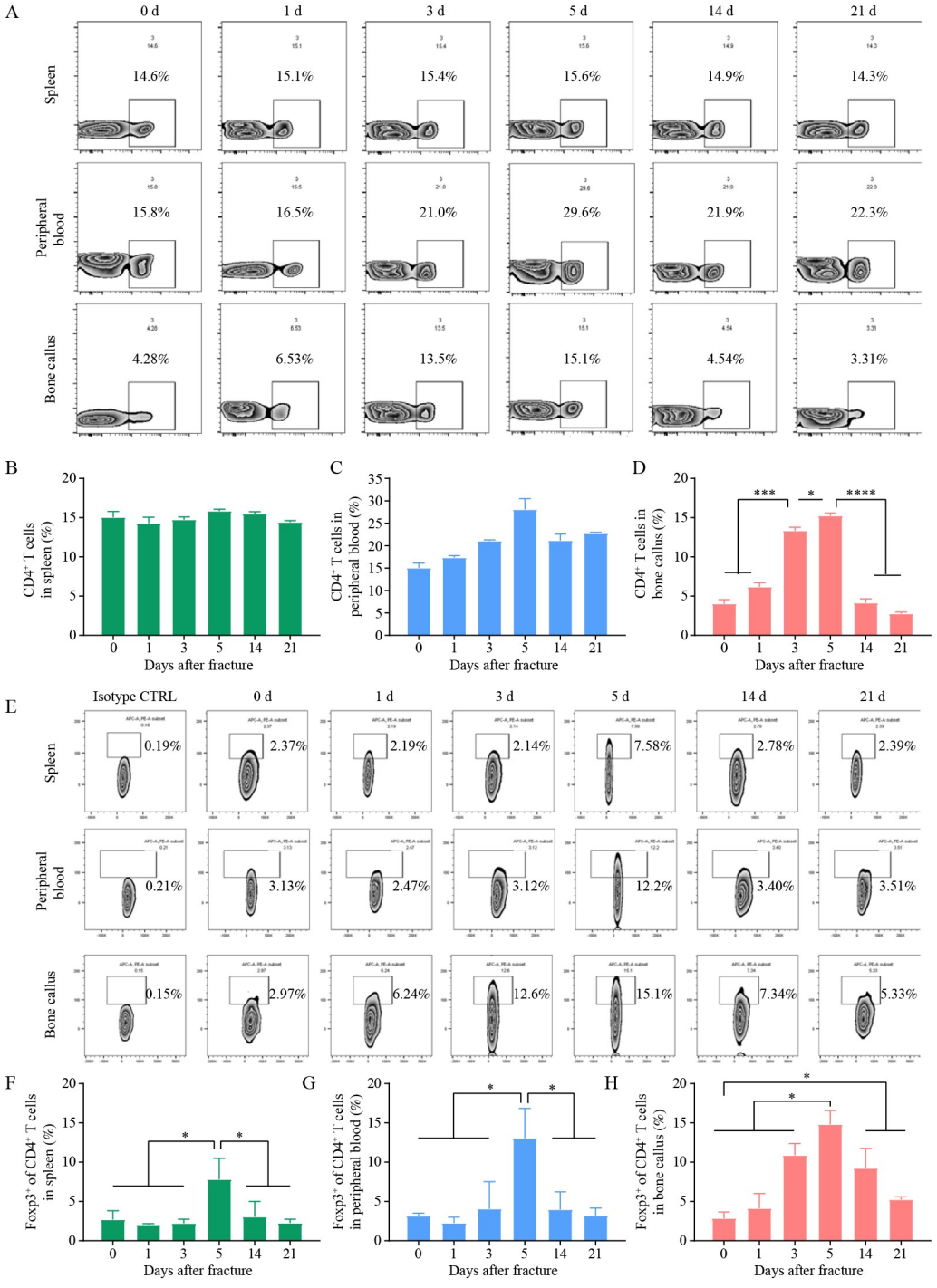

Fig. 1 Treg accumulation in fractured bone. (A) Flow scatter diagram of $CD4^+$ T cells in the spleen, peripheral blood, and bone callus before fracture (day 0) and days 1, 3, 5, 14, and 21 after fracture. Numbers indicate the proportion of cells in the frame. (B–D) Quantitative analysis of $CD4^+$ T cells in the spleen (B), peripheral blood (C), and bone callus (D) at different time points after fracture ($n = 3$). (E) Flow scatter diagram of Tregs in the spleen, peripheral blood, and bone callus before fracture (day 0) and on days 1, 3, 5, 14, and day 21 after. Numbers indicate the proportion of cells in the frame. (F–H) Proportions of Tregs in the spleen (F), peripheral blood (G), and bone callus (H) at different time points after fracture. Five mice were set as one group for all tissues. Data are shown as means ± SD. $*P < 0.05$, $***P < 0.001$, $****P < 0.0001$.

were partially expressed by bone callus Tregs, which suggests that most bone callus Tregs were likely from thymus, and some Tregs may be induced in peripheral tissues (Fig. 2C). Ki67 staining and EdU assay were performed to further investigate the local expansion of Tregs. Ki67 is a commonly used cell proliferation marker and expressed in all phases of the cell cycle except the G0 phase [34]. Five days after fracture, the Tregs in the bone

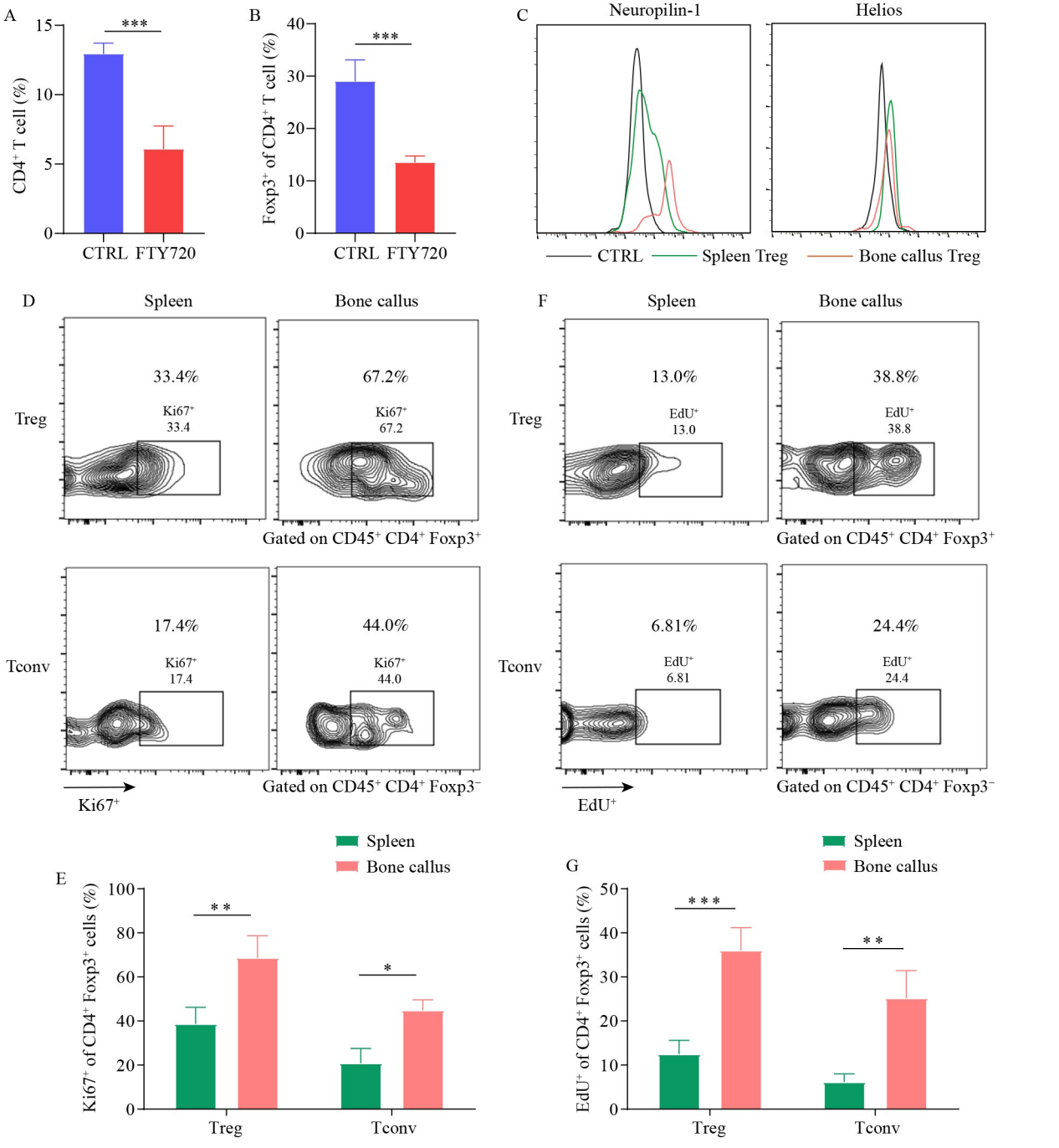

Fig. 2 Sources of Tregs in fractured bone. (A, B) Percentages of $CD4^+$ T cells (A) and Tregs (B) in the bone callus ($n = 4$). FTY720 or solvents were administrated on day 1 before fracture and days 1, 2, 3, and 4 after fracture. Bone callus was collected on day 5 after fracture with the extraction of lymphocytes. (C) Histograms depict the expression of neuropilin-1 and Helios in Tregs from the bone callus and spleen on day 5 post fracture. (D) FCM graphs of Ki67 expression in spleen and bone callus Tregs and Tconvs. Bone callus and spleen were dissected for the analysis 5 days post fracture. Numbers indicate the proportion of cells in the frame. (E) Quantitative analysis of Ki67 in the spleen and bone callus Treg and Tconv cell subsets ($n = 3$). (F) FCM graphs of EdU expression in spleen and bone callus Tregs and Tconvs. Numbers indicate the proportion of cells in the frame. A total of 1 mg EdU was intraperitoneally injected to the mice, and FCM analysis was performed on 24 h post EdU administration. (G) Quantitative analysis of EdU in spleen and bone callus Tregs and Tconvs ($n = 3$). Data are shown as means ± SD. $^*P < 0.05$, $^{**}P < 0.01$, and $^{***}P < 0.001$.

callus and spleen were stained with anti-mouse Ki67 and detected via FCM. Approximately 70% and 40% of bone callus and spleen Tregs were positive for Ki67, respectively and ($P < 0.05$) (Fig. 2D and 2E). DNA replication is essential for cell proliferation. EdU is a thymidine analog that can replace thymine to incorporate

into replicated DNA during the S phase of the cell cycle, which is commonly used to detect DNA replication activity [35]. After 24 h of EdU labeling, EdU^+ cells were detected in about 36% of bone callus Tregs and 12% of spleen Tregs (Fig. 2F and 2G). The proliferation ability of Tconvs ($CD45^+CD4^+Foxp3^-$) was also analyzed. The Tconvs in the bone callus exhibited higher rates of $Ki67^+$ and EdU^+ cells in comparison with the spleen Tconvs. However, the proliferation rate of Tconvs was lower than that of Tregs. The proliferation conditions of Tregs and Tconvs in the spleen and intact bone tissues of normal mice were also detected. As displayed in Fig. S2, approximately 25% and 12% of intact bone Tregs and spleen Tregs were positive for Ki67, respectively; both values were lower than the bone callus Tregs (70%) and spleen Tregs in fractured mice (33%). Tconvs in normal and fractured mice showed similar trends. After 24 h of EdU labeling, EdU^+ cells were detected in 11% of intact bone Tregs and 6% of spleen Tregs, and these values were lower than those in fractured mice. Tconvs presented similar results. Herein, the proliferation of Tregs were remarkably increased after fracture. Collectively, these findings indicate that the bone callus Tregs can be derived from the circulating pool, peripheral induction, and local expansion.

Tregs from bone callus promoted BMSC proliferation and osteogenesis

As Tregs accumulated remarkably in the bone callus, we first intended to demonstrate their role in fracture healing at the cellular level. To evaluate the osteogenesis effect of Treg from different organs, we collected the spleen, non-draining lymph nodes, and bone callus on day 5 after fracture. BMSCs were seeded in 96-well plates, cocultured with these three sources of Tregs directly at a ratio of 5:1, and subjected to EdU assay after 48 h to evaluate their proliferative activity [36]. EdU^+ cells were most prominent in the bone callus Treg-treated group (Fig. 3A and 3C). The total and proliferating cell numbers were both higher in the bone callus Treg-treated group, which suggests that bone callus Treg promoted BMSC proliferation.

Moreover, to investigate the role of Tregs in extracellular matrix mineralization, we seeded BMSCs in 24-well plates and treated them with different Treg sources. Two-week culture of ALP staining was carried out to evaluate the osteogenesis degree. More nitro blue tetrazolium chloride (NBT)-formazan was detected in the bone callus Treg-treated groups, which indicates the enhanced ability for osteogenesis endowed by bone callus Tregs (Fig. 3B and 3D). Collectively, these results demonstrate that Tregs from the bone callus can promote osteogenesis more effectively than those from the spleen and lymph node.

Depletion of Tregs compromised fracture healing

Given that bone callus Tregs promoted osteogenesis *in vitro*, we then performed loss-of-function studies to investigate the role of bone callus Tregs in fracture healing *in vivo*. Treatment with anti-CD25 mAb is a commonly used approach, and it has been studied by researchers to explore the functions of Tregs [37]. Here, we injected 200 μg anti-CD25 mAb or isotype control to C57BL/6 mice intraperitoneally 3 days before and 3 and 4 days after fracture to manipulate the Treg levels. The administration of anti-CD25 did not neutralize the overall Tregs, whether in the spleen, peripheral blood, or bone callus, but it considerably reduced the proportions of CD25. As a result, antibody neutralization in the spleen, peripheral blood, and bone callus depleted 75.6%, 80.5%, and 52.9% of the Tregs, respectively (Fig. S3). Next, we investigated whether Treg depletion compromised fracture healing. We monitored the mice using X-ray imaging on days 1, 3, 5, 7, 14, and 21. Compared with the control group, the antibody-depletion group exhibited markedly increased fracture gap and lower callus volume (Fig. 4A). On day 21 post fracture, the mice were sacrificed, and the fractured femur was dissected and scanned through micro-CT. The 3D reconstructed image of micro-CT showed similar results as the X-ray (Fig. 4B and 4C). We further calculated the bone parameters. As shown in Fig. 4D, the BMD, BV, TV, and BV/TV in the Treg-depletion group were decreased substantially compared with those of the control group. Moreover, AB staining indicated the increased cartilage area at the fracture area of Treg-depletion mice (Fig. S4).

Osteoblast differentiation is critical in bone remolding. Type I collagen (collagen I) is the dominant component of bone organic matrix, and it endows the bone tissue with a high density of collagenous filaments. OCN is a noncollagenous protein synthesized by osteoblasts during bone matrix mineralization [38]. RUNX2, a transcription factor for bone development, plays an important role in osteoblast differentiation and bone formation. To study the effect of Treg depletion on these osteogenic proteins, we used qRT-PCR to measure the mRNA levels in bone callus. Table S1 contains the information on primers. Compared with the control group, considerably lower mRNA levels of these three proteins were detected in the anti-CD25 mAb-treated group (Fig. 4E). These results indicate that the ablation of Tregs compromises fracture healing.

Bone callus Tregs displayed distinct TCR repertoire and transcriptome

Single-cell sequencing was performed to exploit the possible components of bone callus Tregs that promote fracture healing. Limited by the amount of Tregs, $CD4^+$ T

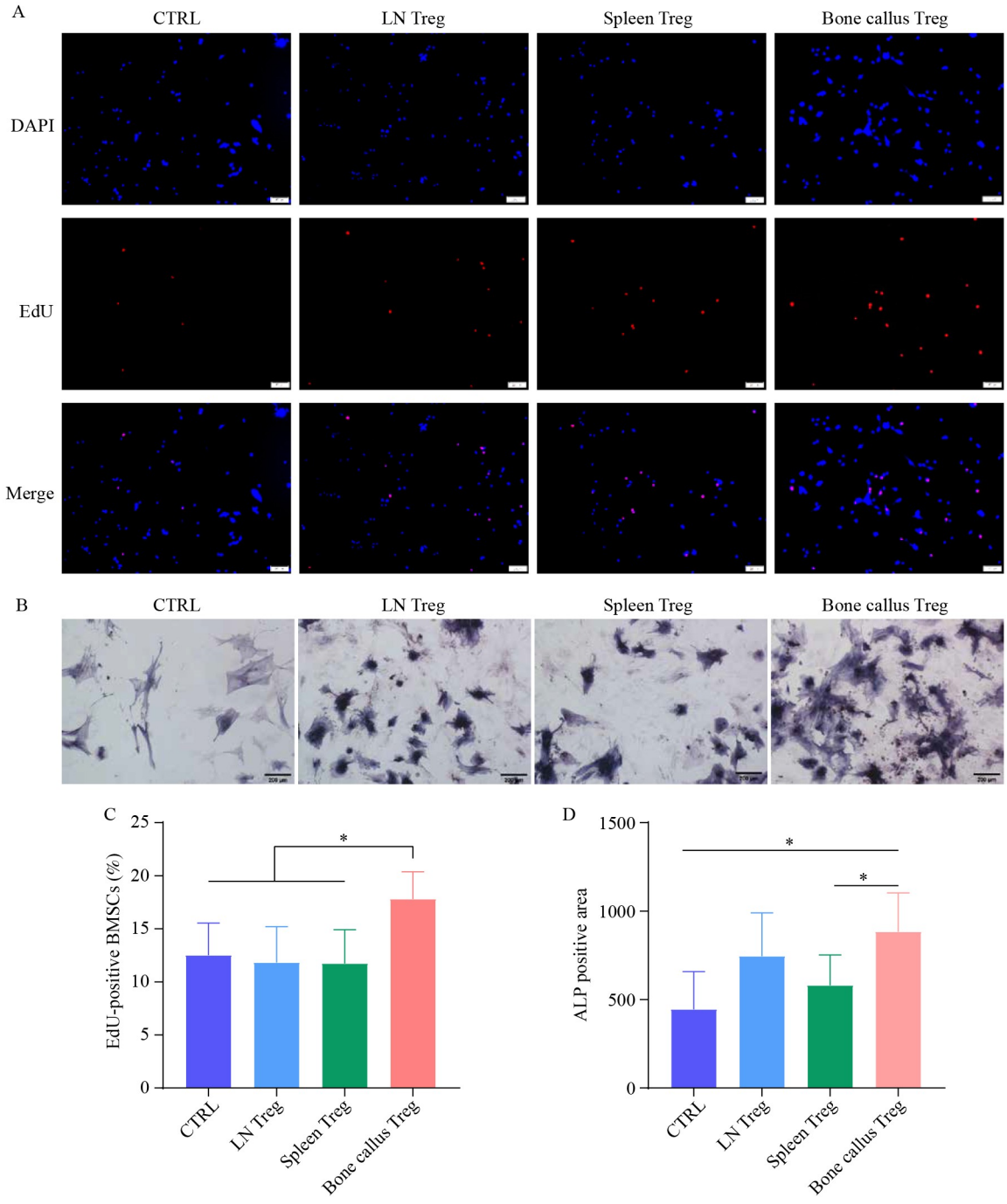

Fig. 3 Tregs from bone callus promoted BMSC proliferation and osteogenesis. (A) Proliferation of BMSCs cultured with different sources of Tregs was tested via EdU assay. The higher the proportion of red dots, the more proliferative the cells. Scale bar = 200 μm. (B) ALP staining of BMSCs in different treatments after culturing with osteogenic induction medium for 14 days. Scale bar = 200 μm. (C) Quantification analysis of the percentage of EdU^+ cells (n = 5). (D) Quantitative analysis of ALP-positive area calculated using ImageJ software (n = 5). Data are shown as means ± SD. *, $P < 0.05$.

cells were sorted for sequencing. Unsupervised cell clustering was performed using Seurat, and Louvain modularity optimization algorithm was used to cluster cell populations. The cluster map of $CD4^+$ T cells was visualized through t-SNE [39]. In addition, the clusters of spleen and bone callus Tregs were identified through the specific gene expression of Foxp3 (Fig. 5A). To investigate the characteristics of clonal restriction, we studied the TCR repertoires by sequencing the CDR 3 of the TCR α and TCR β chains of single cells. A total of 420 and 321 TCR sequences were observed for spleen and bone callus Tregs, respectively. The spleen and bone

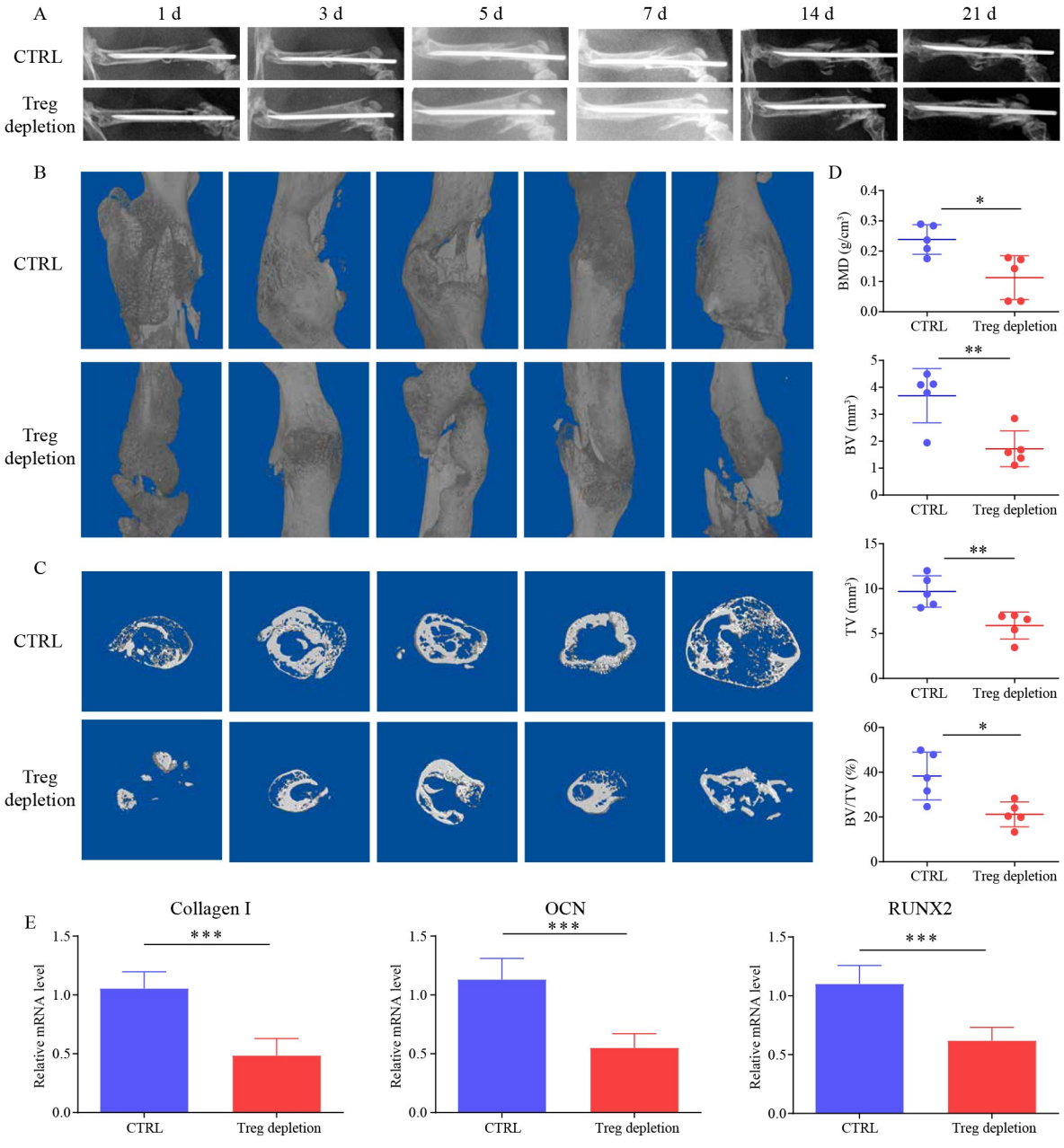

Fig. 4 Depletion of Tregs compromised fracture healing. (A) X-Ray image of fractured mice. On days 1, 3, 5, 7, 14, and 21, the mice were anesthetized using 0.3% pentobarbital (w/v) and scanned via X-ray. (B, C) Micro-CT three-dimensional reconstructed images of the fractured femur on day 21 post fracture. The mice were sacrificed, and the femur was separated for micro-CT scanning. Four mice were included in each group. (D) Calculated BMD, TV, BV, and BV/TV for each group (n = 5). The ROIs were selected as areas 1 mm above and below the fracture gap. (E) mRNA levels of osteogenesis-related proteins (collagen I, OCN, and RUNX2) in bone callus (n = 5). Mice were sacrificed on day 21 post fracture, and the bone callus was analyzed via qRT-PCT. Data are shown as means ± SD. *, $P < 0.05$; **, $P < 0.01$; ***, $P < 0.001$.

callus Tregs had no shared TCR sequences, which indicates the distinct TCR repertoire of the latter. Moreover, a fraction of bone callus Tregs was clonally expanded, which corresponded to the above expansion ability of Tregs (Fig. 5B).

Then, the gene expressions in spleen and bone callus Tregs were analyzed for comparison. Gene set enrichment analysis (GSEA) shows that the enrichment of upregulated genes in bone callus Tregs in Gene Ontology biological process terms, including skeletal muscle tissue regeneration, regeneration, regulation of cell population proliferation, and multicellular organism development, which are related to tissue repair (Fig. 5C). The upregulated genes were further analyzed. The first group of genes (*Rora*, *Gna13*, *Hif1a*, and *Ninj1*) contributes to angiogenesis. The second group included *GZMB*, *Nfkbid*, *Nfkbiz*, *il10*, *ifngr1*, and *tnfrsf9* and participated in the inflammatory effect after injury. The third group

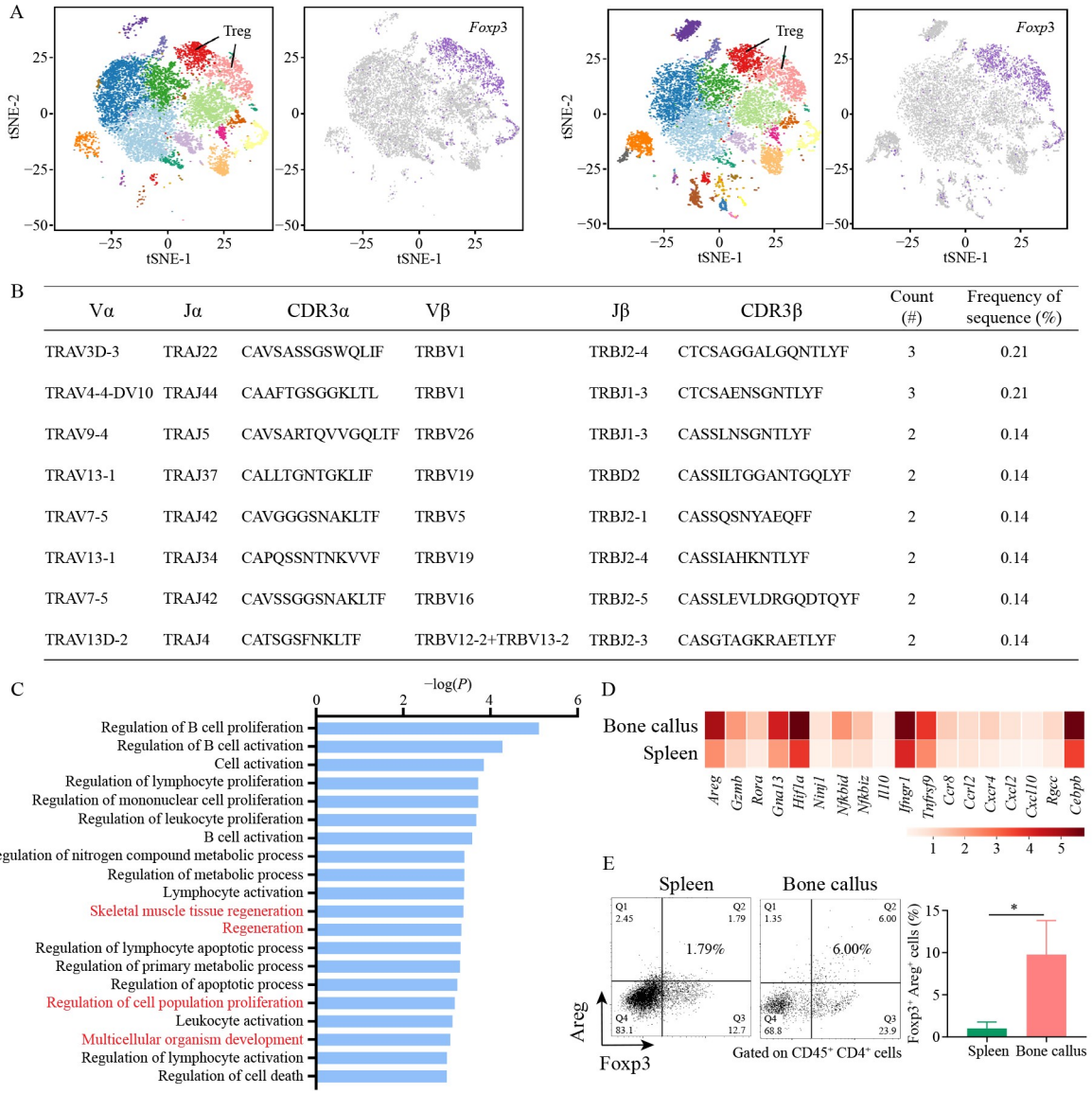

Vα	Jα	CDR3α	Vβ	Jβ	CDR3β	Count (#)	Frequency of sequence (%)
TRAV3D-3	TRAJ22	CAVSASSGSWQLIF	TRBV1	TRBJ2-4	CTCSAGGALGQNTLYF	3	0.21
TRAV4-4-DV10	TRAJ44	CAAFTGSGGKLTL	TRBV1	TRBJ1-3	CTCSAENSGNTLYF	3	0.21
TRAV9-4	TRAJ5	CAVSARTQVVGQLTF	TRBV26	TRBJ1-3	CASSLNSGNTLYF	2	0.14
TRAV13-1	TRAJ37	CALLTGNTGKLIF	TRBV19	TRBD2	CASSILTGGANTGQLYF	2	0.14
TRAV7-5	TRAJ42	CAVGGGSNAKLTF	TRBV5	TRBJ2-1	CASSQSNYAEQFF	2	0.14
TRAV13-1	TRAJ34	CAPQSSNTNKVVF	TRBV19	TRBJ2-4	CASSIAHKNTLYF	2	0.14
TRAV7-5	TRAJ42	CAVSSGGSNAKLTF	TRBV16	TRBJ2-5	CASSLEVLDRGQDTQYF	2	0.14
TRAV13D-2	TRAJ4	CATSGSFNKLTF	TRBV12-2+TRBV13-2	TRBJ2-3	CASGTAGKRAETLYF	2	0.14

Fig. 5 Bone callus Tregs displayed distinct TCR repertoire and transcriptome. (A) Left, t-SNE projection of spleen CD4$^+$ T cells displaying the main cell clusters. The purple dots denote the Treg clusters. Each dot represents a single cell, and each color indicates a different cluster. CD4$^+$ T cells were sorted via FCM on day 5 post fracture, with the cell number reaching 10591. Right, t-SNE projection of bone callus CD4$^+$ T cells and Foxp3$^+$ Tregs, with the cell number reaching 9916. (B) Identical paired CDR3 α and CDR3 β sequences in bone callus Tregs. (C) GSEA revealing the Gene Ontology enrichment of the biological process category in bone callus Tregs *vs* spleen Tregs. The top 20 pathways are listed and ranked by normalized enrichment score. (D) Heat map of selected differential genes between bone callus and spleen Tregs. Averaged from three independent experiments. (E) Cytofluorometric analyses of amphiregulin in bone callus and spleen Tregs (n = 4). Data are shown as means ± SD. *, $P < 0.05$. Areg indicated as amphiregulin in the graphs.

comprised chemokines and chemokine receptor-related genes (e.g., *ccr8*, *cxcl10*, *ccrl2*, *ccr7*, *cxcr4*, and *cxcl2*) and can mediate the recruitment of immune cells. The osteoblast differentiation-related gene *Cebpb* was also upregulated. The well-known growth factor amphiregulin-encoding gene *Areg* exhibited the highest differential expression among these genes (Fig. 5D). FCM analysis was further conducted to confirm the expression of amphiregulin at the protein level. Bone callus Tregs displayed remarkably higher expression of amphiregulin than those of the spleen, lymph node, and intact bone (Figs. 5E, S5, and S6).

Amphiregulin promoted proliferation and osteogenesis of BMSCs

Given that amphiregulin is highly expressed in bone callus Tregs compared with those in spleen and lymph node, we explored whether amphiregulin is the critical factor in Tregs that promotes fracture healing. Initial

examinations focused on the influences of amphiregulin on the proliferation and osteogenesis of BMSCs. For cell proliferation assay, EdU staining was performed on BMSCs treated with different concentrations of amphiregulin (0 ng/mL as the control and 1 ng/mL to 2.5 ng/mL for test). The proliferative effect of amphiregulin worked in a concentration-dependent manner (Fig. 6A and 6B). However, the BMSCs

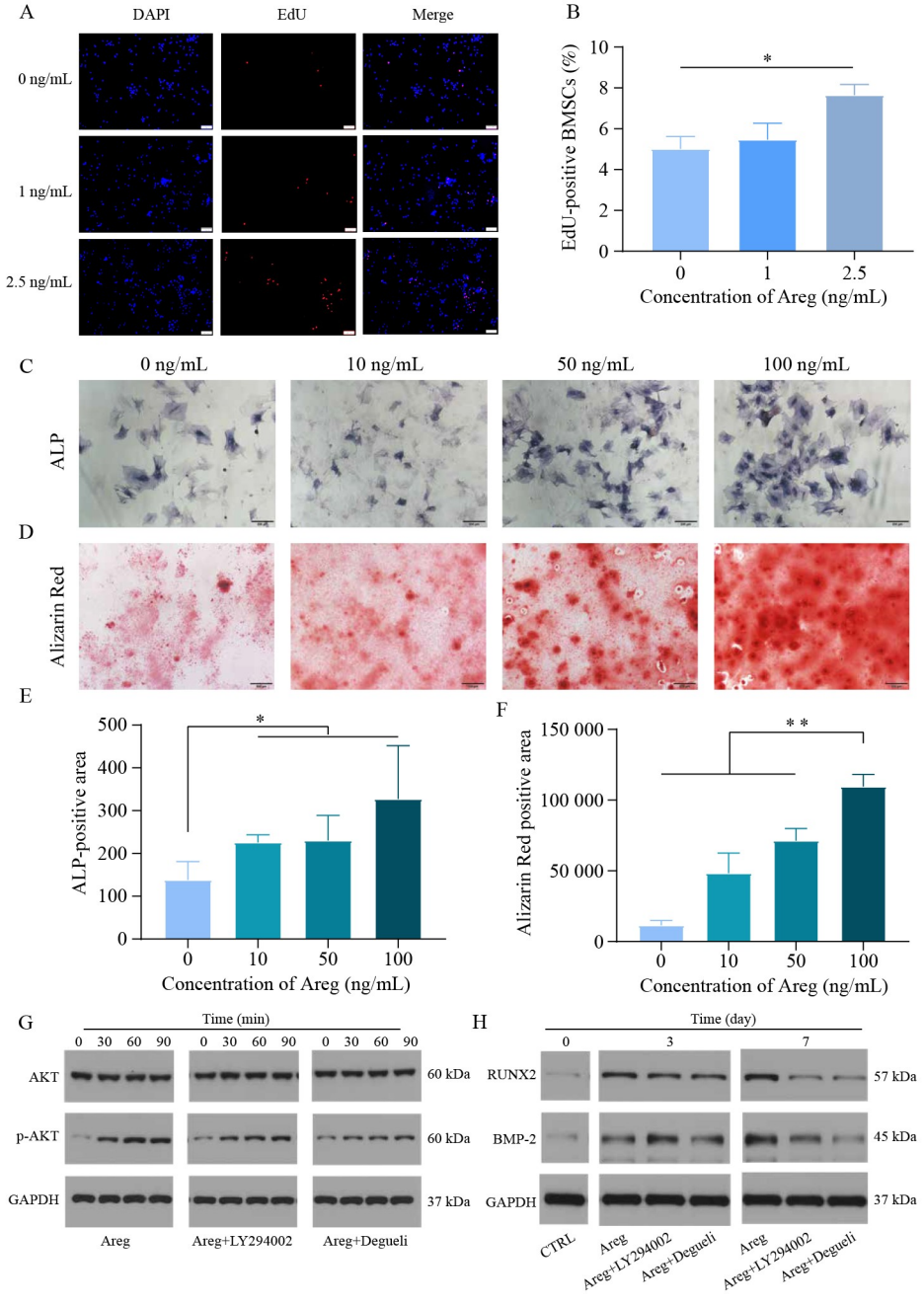

Fig. 6 Amphiregulin promoted proliferation and osteogenesis of BMSCs. (A) After the treatment with different concentrations of amphiregulin from 0 ng/mL to 2.5 ng/mL, EdU assay was performed in 48 h. Scale bar = 200 μm. (B) Quantification analysis of the percentage of EdU-positive cells (n = 5). (C) ALP staining of BMSCs treated with different concentrations of amphiregulin from 0 ng/mL to 100 ng/mL after culturing with osteogenic induction medium for two weeks. (D) Alizarin Red staining of BMSCs treated with different concentrations of Areg from 0 ng/mL to 100 ng/mL after culturing with osteogenic induction medium for six weeks. (E) Quantitative analysis of ALP-positive area calculated using ImageJ software (n = 5). (F) Quantitative analysis of Alizarin Red-positive area calculated using ImageJ software (n = 5). (G) Protein levels of AKT and p-AKT in BMSCs treated with amphiregulin with or without the PI3K inhibitor LY294002 and AKT inhibitor deguelin at different time points (0, 30, 60, and 90 min). (H) Protein expressions of osteogenic markers RUNX2 and BMP-2 (0, 3, and 7 days). Data are shown as means ± SD. *, $P < 0.05$; **, $P < 0.01$. Areg indicated as amphiregulin in the graphs.

exhibited a relatively low expansion ability given the weak fluorescence of cell nuclei. We further conducted CCK-8 assay to evaluate cell proliferation. The results accorded with those of EdU assay, but the low concentrations were not as sensitive as that of EdU owing to the restricted expansion ability of BMSCs and sensitivity of CCK-8 assay. Cell proliferation showed considerable changes when the concentration went up to 5 ng/mL (Fig. S7). Herein, a high concentration of amphiregulin was selected for the following experiments.

To investigate the extracellular matrix mineralization by amphiregulin, we treated BMSCs seeded in 24-well plates with different concentrations of amphiregulin (0, 10, 50, and 100 ng/mL) and continuously cultured them for 2 weeks for ALP staining and 3 weeks for Alizarin Red staining. As shown in Fig. 6C–6F, amphiregulin also worked in a concentration-dependent manner with the most evident osteogenesis effect at 100 ng/mL [40]. Compared with the control group, more dark-blue NBT-formazan and red mineralized nodules were observed in the amphiregulin-treated groups.

The PI3K/AKT signaling pathway plays an important role in various cell functions. Several studies have proven its involvement in osteogenesis and osteoclastogenesis [41,42]. Here, BMSCs were treated with 50 ng/mL amphiregulin. As shown in Fig. 6G, the expression of p-AKT was increased with prolonged incubation, and this effect can be inhibited by the PI3K inhibitor LY294002 and the AKT inhibitor deguelin. Similarly, amphiregulin remarkably upregulated the expressions of osteogenic markers RUNX2 and BMP-2 in BMSCs after treatment for 7 days. The PI3K/AKT signaling pathway inhibitors counteracted this effect (Fig. 6H). Figure S8 shows the original Western blots of Fig. 6G and 6H. We also explored whether the mitogen-activated protein kinase (MAPK)/extracellular signal-regulated kinase (ERK) pathway was also involved in the amphiregulin-mediated osteogenesis of BMSCs (Fig. S9). However, the amphiregulin treatment did not increase the expression of phosphorylated ERK, which suggests the possible negligible effect of amphiregulin on the MAPK/ERK pathway. These findings indicate that the PI3K/AKT pathway can be mainly involved in amphiregulin-induced differentiation of BMSCs.

Amphiregulin reversed the compromised healing caused by Treg depletion

The above findings prove the positive effect of amphiregulin on the proliferation and osteogenesis of BMSCs. The effect of amphiregulin on fracture healing *in vivo* was explored. The mice were treated following the protocol in Fig. 7A, and X-ray photography was used to observe the real-time process of fracture healing. The callus was the largest in amphiregulin-treated groups but the smallest in Treg-depletion groups (Fig. 7B). Direct observation and comparison of the calluses obtained on day 21 after fracture revealed that callus formation was more pronounced in amphiregulin-treated groups, and the ablation of Tregs resulted in reduced callus formation (Fig. S10). By comparing the sizes of calluses, we preliminarily concluded that amphiregulin benefitted fracture healing, and the ablation of Tregs compromised the healing process. Micro-CT analysis was further conducted, with the three-dimensional images presenting better results in fracture healing conditions in the amphiregulin-treated groups (Fig. 7C). In addition, remarkable improvements were observed in the bone metabolism-related indexes (BMD, BV, TV, and BV/TV) of the two amphiregulin-treated groups compared with those of the isotype control or anti-CD25 treated groups (Fig. 7D). Furthermore, the level of OCN, a marker for bone formation evaluation [43], confirmed the osteogenesis effect of amphiregulin (Fig. 7E). However, a similar trend was not observed in the measurement of serum ALP (Fig. 7F), which may be related to a wide range of ALP sources [44]. We then detected the concentration of bone-derived ALP (B-ALP). As displayed in Fig. 7G, amphiregulin-treated groups showed higher B-ALP levels than the control groups. Bone samples were also acquired for histological evaluation and immunohistochemical analysis. According to the results of H&E and AB staining, the amphiregulin-treated groups showed an increased number of bone trabecula and a reduced cartilage area. In addition, more TRAP-positive cells were found in the amphiregulin-treated groups, which indicates that amphiregulin accelerated the bone remolding phase [45,46] (Fig. 7H). Furthermore, to investigate the *in vivo* effect of amphiregulin on the PI3K/AKT pathway, we examined the protein expressions of AKT, p-AKT, RUNX2, and BMP-2 in the fracture microenvironment through Western blotting. Consistent with cell experiments, *in vivo* amphiregulin treatment increased the phosphorylation of AKT and the expressions of osteogenic markers RUNX2 and BMP-2 (Figs. S11 and S12), which imply that amphiregulin promotes fracture repair through the activation of the PI3K/AKT pathway.

Exploration of amphiregulin for human fracture healing

At the animal level, we have proven that Tregs can promote fracture healing, and this effect can be mediated by amphiregulin. To explore whether Treg and amphiregulin exert similar effects in patients, we analyzed the changes in Tregs in human bone callus and investigated the role of amphiregulin in hUC-MSCs. Bone callus and peripheral blood were collected by operators. Table S2 displays the clinical and demographic

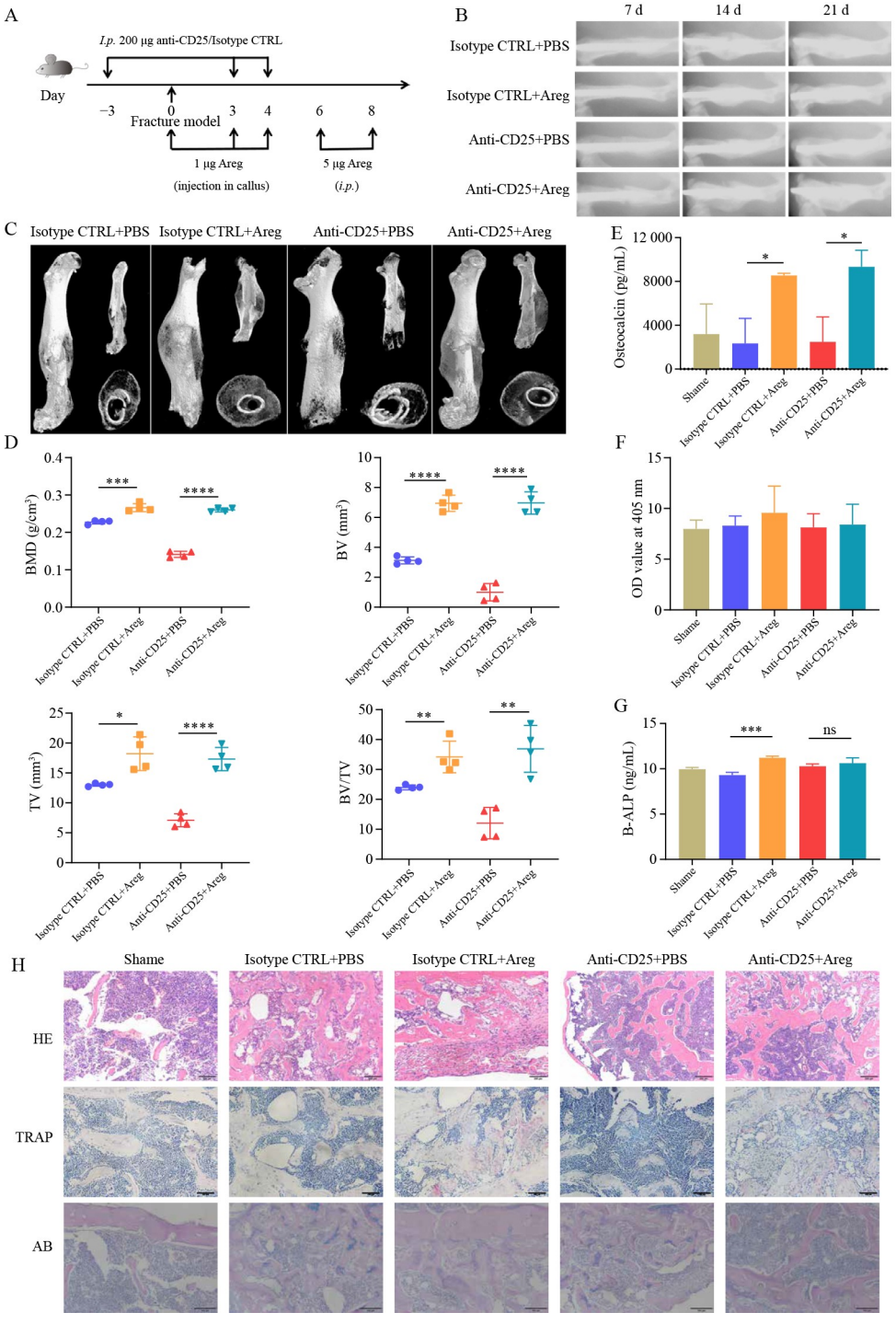

Fig. 7 Amphiregulin reversed the compromised healing caused by Treg depletion. (A) Mouse model and administration protocol. (B) X-Rays images of fracture healing process among different groups on days 7, 14, and 21 post fracture. The mice were anesthetized via injection of sodium pentobarbital to capture X-ray images. (C) Micro-CT three-dimensional reconstructed images of fractured femur on day 21 post fracture. The mice were sacrificed, and the femur was separated for micro-CT scanning. Four mice were included in each group. (D) Calculated BMD, TV, BV, and BV/TV in each group ($n = 5$). The ROIs were selected as areas 1 mm above and below the fracture gap. (E–G) Serum levels of OCN (E), ALP (F), and B-ALP (G) in different groups ($n = 3$). (H) Representative histological evaluation of callus formation on day 21. The calluses were stained with H&E/TRAP/AB. Scale bar for HE and TRAP = 200 μm; scale bar for AB = 100 μm. Data are shown as means ± SD. *, $P < 0.05$; **, $P < 0.01$; ***, $P < 0.001$; and ****, $P < 0.0001$. Areg indicated as amphiregulin in the graphs.

details of the 30 fractured patients. The results on white blood cells, monocytes, and lymphocytes revealed that all patients were free of infection. Other baseline characteristics, including gender, age, bodyweight, and

sample collection time, showed no remarkable differences between the two groups of patients for peripheral blood and bone callus collection, respectively. Lymphocytes were separated from the collected tissues and analyzed through FCM. Compared with peripheral blood, the fractured callus presented higher expressions of $CD4^+$ T cells (Fig. 8A and 8B) and Tregs (Fig. 8C and 8D). The Tregs in the bone callus and peripheral blood were sorted through FCM, and amphiregulin expression was analyzed via qRT-PCR. Table S3 displays the clinical and demographic details of the 16 fractured patients. Compared with blood Tregs, bone callus Tregs showed a notably higher expression of amphiregulin (Fig. 8E).

Furthermore, the effect of amphiregulin on the proliferation and osteogenesis of hUC-MSCs was monitored through EdU assay and ALP/Alizarin Red staining. Similar with that of BMSCs, the proliferative effect of amphiregulin occurred in a concentration-dependent manner (Fig. 8F–8J). As for osteogenic effect, the higher the concentration of amphiregulin, the more evident the outcomes of osteogenesis. Therefore, the positive influence of amphiregulin on osteogenesis also applied to the hUC-MSCs. Fracture healing is a regeneration process that includes stem cell differentiation, osteogenesis, chondrogenesis, and angiogenesis. Human umbilical vein endothelial cells (HUVECs) are a widely available source for conducting angiogenesis-related experiments, and their proliferation positively affects angiogenesis [47,48]. Here, for HUVECs treated with amphiregulin from 0 ng/mL to 2.5 ng/mL for 48 h, more EdU-positive cells were observed in the higher-concentration groups than in the control groups. CCK-8 assay indicated a similar trend (Fig. S13). Herein, in addition to promoting osteogenic differentiation of stem cells, amphiregulin may exert angiogenetic roles, which benefits fracture healing from the aspect of vascular repair [49].

Discussion

Fracture is a common and costly burden caused by bone injury or diseases; it may induce severe fracture-related pain, abnormal stump movement, deformity, and loss of function [50,51]. On average, most fractures heal normally within 3–6 months under usual treatments. However, 5%–10% of fractures fail to heal appropriately and cause remarkable negative consequences in the life quality and functional status of individuals [52]. The treatments of delayed healing or nonunion mainly depend on surgery, addition or replacement of internal fixation, bone transplantation, etc., and surgery is not only traumatic but also has the risk of nonunion [53]. In addition, some nonsurgical treatments, including physical therapy and traditional Chinese medicine, are subeffective given their long treatment cycle and individual differences [54]. Herein, the exploration of novel therapeutic targets to promote fracture healing benefits the reduction of pain felt by patients and alleviation of economic and social burden. In recent decades, immune system has been reported to modulate the fracture healing process. Immediately after fracture, platelets arrive at the injured site and create the fibrin thrombus [55]. Neutrophils also contribute to the fibrin thrombus by depositing a fibronectin matrix at the early stage of inflammatory phase [56] and participating in the removal of cellular and tissue debris at the later stage [57]. The roles of macrophages in the fracture healing process differ depending on the subsets. M1 macrophages can clear necrotic cells and fibrin thrombi during the initial acute-inflammation phase, but they exacerbate inflammation and tissue necrosis [58]. M2 macrophages secrete cytokines and factors (e.g., IL-10, TGF-β, IL-4, and vascular endothelial growth factor to alleviate inflammation and promote tissue regeneration [59]. T and B lymphocytes can play a cell-signaling role in the healing process [60]. These cells are relatively well-characterized immune cell types, but other new immunotherapeutic targets remain poorly understood. Moreover, these cells regulate healing process mainly based on their immunological effects. Tregs can also regulate fracture healing through their immunological roles, especially through cytokine secretion. Tregs inhibit osteoclast differentiation and bone resorption by secreting TGF-β [61]. They can also express other cytokines, such as granulocyte-macrophage colony-stimulating factor and IL-5 IL-10, that inhibit osteoclast differentiation [62]. Moreover, Tregs can induce new bone formation by secreting IL-10 [63]. Whether extraimmunological roles are involved in the healing process remains elusive. Inspired by the findings on the unique repair role of Tregs in tissue injury (e.g., muscle, heart, and lung), we speculated whether the Tregs in fractured bone may perform a distinct role in the healing process and designed a series of experiments to evaluate their possible functions.

The changes in Tregs in the callus of injured bone, peripheral blood of the systemic circulation, and spleen of lymphoid organs were first analyzed. Tregs specifically express the transcription factor Foxp3 in the nucleus and CD25 and CTLA-4 on the cell surface. Foxp3, which is the most sensitive maker of Tregs, is required for Treg function, especially suppressive activities. $CD4^+Foxp3^+$ has been used to identify Tregs from the peripheral blood, spleen, lung, and axillary and inguinal and mesenteric lymph nodes and from large intestine lamina propria [11,64]. Therefore, here, we used $CD45^+CD4^+Foxp3^+$ to identify Tregs. Compared with the Tregs in peripheral blood and spleen, the Tregs in the bone callus were

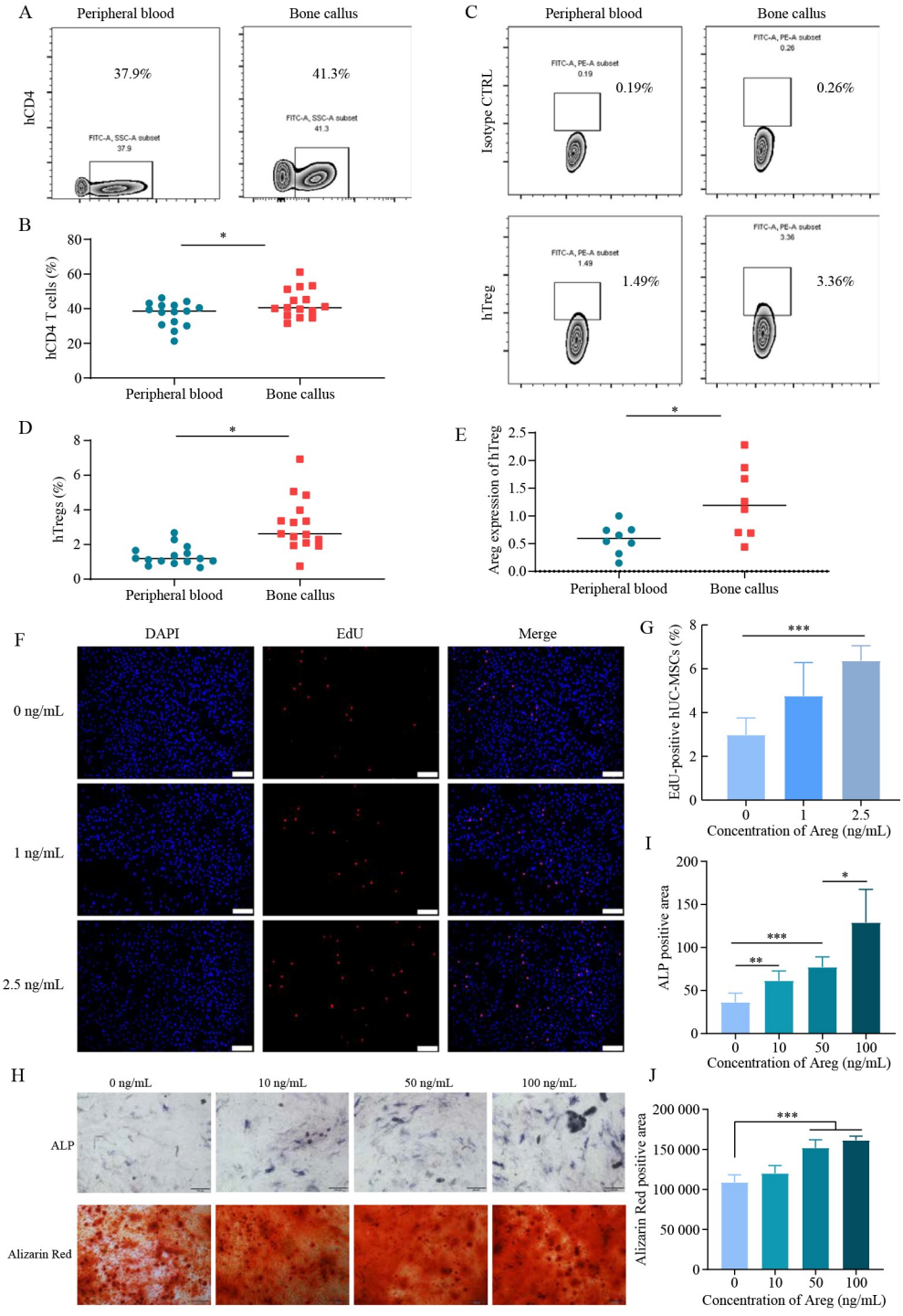

Fig. 8 Exploration of amphiregulin for human fracture healing. (A) Flow scatter diagrams of human $CD4^+$ T ($hCD4^+$ T) cells in peripheral blood and bone callus of fracture patients. Numbers indicate the proportion of cells in the frame. (B) Proportions of $hCD4^+$ T cells in peripheral blood and bone callus of fracture patients (n = 15). (C) Flow scatter diagram of Tregs (hTregs) in peripheral blood and bone callus of fracture patients. Numbers indicate the proportion of cells in the frame. (D) Proportions of hTregs of fracture patients (n = 15). (E) mRNA levels of amphiregulin in blood and bone callus Tregs (n = 8). (F) EdU assay of hUC-MSCs treated with different concentrations of amphiregulin for 48 h. Scale bar = 200 μm. (G) Quantification analysis of the percentage of EdU-positive cells (n = 5). (H) ALP and Alizarin Red staining of hUC-MSCs treated with different concentrations of amphiregulin. Scale bar = 100 μm. (I,J) Quantitative analysis of ALP and Alizarin Red-positive area calculated using ImageJ software (n = 5). Data are shown as means ± SD. *, $P < 0.05$; ***, $P < 0.001$. Areg indicated as amphiregulin in the graphs.

considerably increased after fracture. The accumulation of Tregs in injured bone implies their possible role in the subsequent healing process. EdU staining was performed to investigate the source of Tregs, thymus cell markers,

FTY720, and Ki67. The results show that bone callus Tregs were not totally derived from thymus and may be partially induced in peripheral tissues. Circulatory Tregs can be rapidly recruited to the injured area upon tissue damage or injury [65]. Tregs in the peripheral blood, which can also be a source of the enriched Tregs in the fracture area, were remarkably increased after fracture. After preventing the departure of lymphocytes from secondary lymphoid tissue to the systemic circulation using FTY720, the numbers of $CD4^+$ T cells and Tregs in bone callus were greatly decreased, which indicates that a few bone callus Tregs originated from the circulating pool. For cell expansion assay, the bone callus Tregs and Tconvs showed more excellent proliferation abilities than those in the spleen. The local expansion of Tregs can also be a source of bone callus Tregs. Thus, to directly verify the distinct role of Tregs in the bone callus, we used FCM to sort Tregs from different tissues. Compared with Tregs from the spleen and nondraining lymph node, the bone callus Tregs markedly promoted the proliferation and differentiation of BMSCs toward osteogenesis. The results indicate that bone callus Tregs, rather than the Tregs in lymphoid organs, displayed unique functions. Furthermore, the loss-of-function experiment was carried out through the administration of anti-CD25 mAb to the experimental mice. Tregs in the spleen, peripheral blood, and bone callus cannot be fully depleted but were all neutralized considerably. The depletion of Tregs compromised the effective fracture healing. All the mice in the isotype control group healed normally after 21 days. However, those in the Treg-depleted group showed delayed healing, with nonunion occurring in 60% of the mice (3/5), which proves the prohealing roles of Tregs.

Single-cell sequencing can be used to accurately measure the gene structure and expression state of a single cell to analyze the heterogeneity of cells with the same phenotype [66]. Here, we sorted $CD4^+$ T cells from the bone callus and spleen and conducted single-cell sequencing. Foxp3-expressing cells were determined as Tregs for further analysis. The t-SNE images of bone callus and spleen Tregs were similar. However, the callus Tregs had distinct TCR repertoires and shared no TCR sequences with the spleen Tregs. The upregulated gene expressions of bone callus Tregs were further enriched by Gene Ontology biological process terms. Four biological processes concerning tissue regeneration were involved in the top 20 biological processes. Five groups of typical genes were determined. The group of chemokines contributes to the recruitment of Tregs to injured bone, and that of cytokines plays a role in the regulation of inflammatory response. A group of genes related to angiogenesis was also upregulated and contributes to the repair of implicated skeletal muscle. Cebpb, the gene encoding CCAAT/enhancer-binding protein beta and which can facilitate the maturation of chondrocytes and differentiation of osteoblasts, was also upregulated [67]. Notably, *Areg* was the most differentially upregulated gene. *Areg* encodes amphiregulin protein, which is a member of epidermal growth factor (EGF) family and sends signals through the EGF receptor (EGFR) system. The expression of amphiregulin at the protein level was also verified via FCM analysis. Bone callus Tregs showed the highest level of amphiregulin compared with those in the spleen and intact bone tissues. Reports have suggested that most hematopoietic cell-types express no or low levels of *Areg* transcripts; in addition, *Areg* is not expressed at significant levels in nonhematopoietic cell types [10]. Different from other EGF members that primarily function in cell proliferation, amphiregulin cannot only induce mitotic signals for proliferation but also promote cell differentiation [68]. In regard to bone regeneration, the most important process is the differentiation of MSCs to osteoblasts. EGFR is expressed by various cells, including those of mesenchymal lineages [69]. Herein, the specific properties of amphiregulin may provide an extraimmunological option for bone callus Tregs to participate in bone repair. To validate our assumptions, we directly incubated amphiregulin with BMSCs. The results demonstrate that amphiregulin can promote the proliferation and osteogenesis differentiation of BMSCs. We also performed loss- and gain-function studies to evaluate the *in vivo* prohealing effect of amphiregulin. The administration of recombinant amphiregulin can reverse the compromised fracture healing caused by Treg depletion. PI3K/AKT-related pathways are widely studied in the investigation of osteogenesis. *In vivo* and *in vitro* results suggest that amphiregulin is functionalized through the activation of AKT phosphorylation. These results indicate that bone callus Tregs can promote BMSC differentiation toward osteogenesis via the action of amphiregulin to promote fracture healing (Fig. 9).

We have demonstrated the distinct "repair" role of bone callus Tregs in fracture at the animal level. Notably, we conjectured whether a similar phenomenon can be observed in fracture patients. Bone callus and peripheral blood were collected during surgery and analyzed via FCM. Similar to the findings of animal experiments, bone callus Tregs were remarkably elevated after fracture. As the clinical application of amphiregulin has not been approved, hUC-MSCs were used in the *in vitro* analysis. Amphiregulin can also effectively improve the proliferation and osteogenic differentiation of hUC-MSCs. Moreover, amphiregulin can promote the proliferation of HUVECs, which indicates its possible role in angiogenesis.

This study encountered some limitations. First, a larger clinical sample size of fractured patients is necessary for

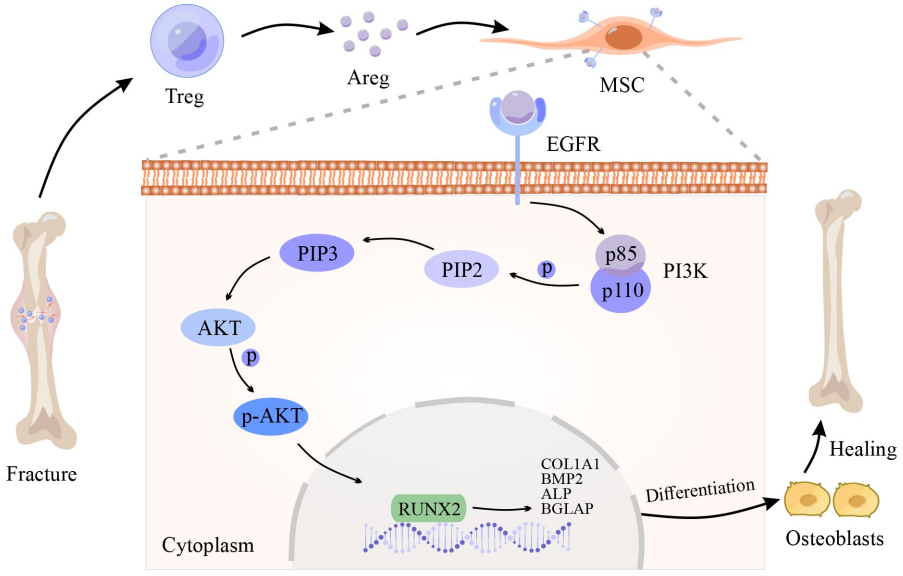

Fig. 9 Proposed mechanism of Treg-mediated fracture healing process. PIP2, phosphatidylinositol 4,5-bisphosphate; PIP3, phosphatidylinositol 3,4,5-trisphosphate; BGLAP, osteocalcin.

more validated clinical results. Second, the results of animal experiments may be inconsistent with those of human trials because of the physiological differences between humans and animals. However, owing to the restriction of study approvement, we cannot obtain *in vivo* results regarding the influence of Tregs or amphiregulin on human fracture healing. Lastly, numerous studies have demonstrated the application potential of Tregs in human, but multiple clinical trials have not been performed yet. The market of Treg is promising. However, Treg therapy is still in a relatively early stage with most candidates in preclinical or early-stage clinical trials. In addition, the side effects of Treg therapy, such as unknown cytokine interactions, can be unexpected owing to the complexity of the immune system.

In summary, we identified the distinct functions of Tregs in bone callus and their critical products in fracture healing. The bone callus Tregs were enriched in the injured bone area. The circulation pool, peripheral induction, and local cell expansion can contribute to Treg accumulation. Moreover, bone callus Tregs showed a higher excellent capacity for osteogenesis than Tregs in lymphoid organs. The depletion of Tregs compromised fracture healing. Amphiregulin was highly overexpressed by bone callus Tregs and can reverse the delayed healing caused by Treg depletion. In addition, amphiregulin mediated osteogenesis via the activation of the PI3K/AKT signaling pathway. Tregs also showed enrichment in patient bone callus, and amphiregulin improved the osteogenesis of human preosteoblastic cells. Thus, Tregs and their products can emerge as potentially novel therapeutic targets for fracture healing and have the potential for clinical translation.

Acknowledgements

This work was supported by the National Natural Science Foundation of China (Nos. 82274026 and 81901884). We thank the patients and families for donating specimens for research. We acknowledge the central laboratory of Union Hospital for X-ray and microscopes imaging. We appreciate the Analytical and Testing Center of Tongji Medical School, Huazhong University of Science & Technology (HUST) for the micro-CT imaging.

Compliance with ethics guidelines

Conflicts of interest Tingting Wu, Lulu Wang, Chen Jian, Zhenhe Zhang, Ruiyin Zeng, Bobin Mi, Guohui Liu, Yu Zhang, and Chen Shi declare that they have no conflict of interest.

The study was approved by the Institutional Animal Care and Use Committee of Tongji Medical College, Huazhong University of Science and Technology (HUST) and the study was performed in accordance with the ethical standards as laid down in the 1964 *Declaration of Helsinki* and its later amendments or comparable ethical standards. Informed consent was obtained from all patients for being included in the study.

Electronic Supplementary Material Supplementary material is available in the online version of this article at https://doi.org/10.1007/s11684-023-1024-8 and is accessible for authorized users.

References

1. Josefowicz SZ, Lu LF, Rudensky AY. Regulatory T cells: mechanisms of differentiation and function. Annu Rev Immunol 2012; 30(1): 531–564
2. Lei H, Schmidt-Bleek K, Dienelt A, Reinke P, Volk HD.

Regulatory T cell-mediated anti-inflammatory effects promote successful tissue repair in both indirect and direct manners. Front Pharmacol 2015; 6: 184
3. Rothstein DM, Camirand G. New insights into the mechanisms of Treg function. Curr Opin Organ Transplant 2015; 20(4): 376–384
4. Luo CT, Li MO. Transcriptional control of regulatory T cell development and function. Trends Immunol 2013; 34(11): 531–539
5. Roncador G, Brown PJ, Maestre L, Hue S, Martínez-Torrecuadrada JL, Ling KL, Pratap S, Toms C, Fox BC, Cerundolo V, Powrie F, Banham AH. Analysis of FOXP3 protein expression in human $CD4^+CD25^+$ regulatory T cells at the single-cell level. Eur J Immunol 2005; 35(6): 1681–1691
6. Kanamori M, Nakatsukasa H, Okada M, Lu Q, Yoshimura A. Induced regulatory T cells: their development, stability, and applications. Trends Immunol 2016; 37(11): 803–811
7. Burzyn D, Benoist C, Mathis D. Regulatory T cells in nonlymphoid tissues. Nat Immunol 2013; 14(10): 1007–1013
8. Feuerer M, Herrero L, Cipolletta D, Naaz A, Wong J, Nayer A, Lee J, Goldfine AB, Benoist C, Shoelson S, Mathis D. Lean, but not obese, fat is enriched for a unique population of regulatory T cells that affect metabolic parameters. Nat Med 2009; 15(8): 930–939
9. Cipolletta D, Feuerer M, Li A, Kamei N, Lee J, Shoelson SE, Benoist C, Mathis D. PPAR-γ is a major driver of the accumulation and phenotype of adipose tissue Treg cells. Nature 2012; 486(7404): 549–553
10. Burzyn D, Kuswanto W, Kolodin D, Shadrach JL, Cerletti M, Jang Y, Sefik E, Tan TG, Wagers AJ, Benoist C, Mathis D. A special population of regulatory T cells potentiates muscle repair. Cell 2013; 155(6): 1282–1295
11. Arpaia N, Green JA, Moltedo B, Arvey A, Hemmers S, Yuan S, Treuting PM, Rudensky AY. A distinct function of regulatory T Cells in tissue protection. Cell 2015; 162(5): 1078–1089
12. Xia N, Lu Y, Gu M, Li N, Liu M, Jiao J, Zhu Z, Li J, Li D, Tang T, Lv B, Nie S, Zhang M, Liao M, Liao Y, Yang X, Cheng X. A unique population of regulatory T cells in heart potentiates cardiac protection from myocardial infarction. Circulation 2020; 142(20): 1956–1973
13. Deliyanti D, Talia DM, Zhu T, Maxwell MJ, Agrotis A, Jerome JR, Hargreaves EM, Gerondakis S, Hibbs ML, Mackay F, Wilkinson-Berka JL. $Foxp3^+$ Tregs are recruited to the retina to repair pathological angiogenesis. Nat Commun 2017; 8(1): 748
14. Ali N, Zirak B, Rodriguez RS, Pauli ML, Truong HA, Lai K, Ahn R, Corbin K, Lowe MM, Scharschmidt TC, Taravati K, Tan MR, Ricardo-Gonzalez RR, Nosbaum A, Bertolini M, Liao W, Nestle FO, Paus R, Cotsarelis G, Abbas AK, Rosenblum MD. Regulatory T cells in skin facilitate epithelial stem cell differentiation. Cell 2017; 169(6): 1119–1129.e11
15. Baht GS, Vi L, Alman BA. The role of the immune cells in fracture healing. Curr Osteoporos Rep 2018; 16(2): 138–145
16. Wildemann B, Ignatius A, Leung F, Taitsman LA, Smith RM, Pesántez R, Stoddart MJ, Richards RG, Jupiter JB. Non-union bone fractures. Nat Rev Dis Primers 2021; 7(1): 57
17. Zura R, Xiong Z, Einhorn T, Watson JT, Ostrum RF, Prayson MJ, Della Rocca GJ, Mehta S, McKinley T, Wang Z, Steen RG. Epidemiology of fracture nonunion in 18 human bones. JAMA Surg 2016; 151(11): e162775
18. Horton JE, Raisz LG, Simmons HA, Oppenheim JJ, Mergenhagen SE. Bone resorbing activity in supernatant fluid from cultured human peripheral blood leukocytes. Science 1972; 177(4051): 793–795
19. Arron JR, Choi Y. Bone versus immune system. Nature 2000; 408(6812): 535–536
20. Wing K, Onishi Y, Prieto-Martin P, Yamaguchi T, Miyara M, Fehervari Z, Nomura T, Sakaguchi S. CTLA-4 control over $Foxp3^+$ regulatory T cell function. Science 2008; 322(5899): 271–275
21. Bozec A, Zaiss MM. T regulatory cells in bone remodelling. Curr Osteoporos Rep 2017; 15(3): 121–125
22. Cano-Gamez E, Soskic B, Roumeliotis TI, So E, Smyth DJ, Baldrighi M, Willé D, Nakic N, Esparza-Gordillo J, Larminie CGC, Bronson PG, Tough DF, Rowan WC, Choudhary JS, Trynka G. Single-cell transcriptomics identifies an effectorness gradient shaping the response of $CD4^+$ T cells to cytokines. Nat Commun 2020; 11(1): 1801
23. Butler A, Hoffman P, Smibert P, Papalexi E, Satija R. Integrating single-cell transcriptomic data across different conditions, technologies, and species. Nat Biotechnol 2018; 36(5): 411–420
24. Zheng GX, Terry JM, Belgrader P, Ryvkin P, Bent ZW, Wilson R, Ziraldo SB, Wheeler TD, McDermott GP, Zhu J, Gregory MT, Shuga J, Montesclaros L, Underwood JG, Masquelier DA, Nishimura SY, Schnall-Levin M, Wyatt PW, Hindson CM, Bharadwaj R, Wong A, Ness KD, Beppu LW, Deeg HJ, McFarland C, Loeb KR, Valente WJ, Ericson NG, Stevens EA, Radich JP, Mikkelsen TS, Hindson BJ, Bielas JH. Massively parallel digital transcriptional profiling of single cells. Nat Commun 2017; 8(1): 14049
25. Fan X, Dong J, Zhong S, Wei Y, Wu Q, Yan L, Yong J, Sun L, Wang X, Zhao Y, Wang W, Yan J, Wang X, Qiao J, Tang F. Spatial transcriptomic survey of human embryonic cerebral cortex by single-cell RNA-seq analysis. Cell Res 2018; 28(7): 730–745
26. Li J, Tan J, Martino MM, Lui KO. Regulatory T-cells: potential regulator of tissue repair and regeneration. Front Immunol 2018; 9: 585
27. Luckheeram RV, Zhou R, Verma AD, Xia B. $CD4^+$ T cells: differentiation and functions. Clin Dev Immunol 2012; 2012: 925135
28. Zhang C, Li L, Feng K, Fan D, Xue W, Lu J. 'Repair' Treg cells in tissue injury. Cell Physiol Biochem 2017; 43(6): 2155–2169
29. Saxena A, Dobaczewski M, Rai V, Haque Z, Chen W, Li N, Frangogiannis NG. Regulatory T cells are recruited in the infarcted mouse myocardium and may modulate fibroblast phenotype and function. Am J Physiol Heart Circ Physiol 2014; 307(8): H1233–H1242
30. Kunkel GT, Maceyka M, Milstien S, Spiegel S. Targeting the sphingosine-1-phosphate axis in cancer, inflammation and beyond. Nat Rev Drug Discov 2013; 12(9): 688–702
31. Yadav M, Louvet C, Davini D, Gardner JM, Martinez-Llordella M, Bailey-Bucktrout S, Anthony BA, Sverdrup FM, Head R, Kuster DJ, Ruminski P, Weiss D, Von Schack D, Bluestone JA. Neuropilin-1 distinguishes natural and inducible regulatory T cells among regulatory T cell subsets *in vivo*. J Exp Med 2012; 209(10): 1713–1722, s1–19
32. Thornton AM, Korty PE, Tran DQ, Wohlfert EA, Murray PE, Belkaid Y, Shevach EM. Expression of Helios, an Ikaros

transcription factor family member, differentiates thymic-derived from peripherally induced Foxp3$^+$ T regulatory cells. J Immunol 2010; 184(7): 3433–3441
33. Nikolouli E, Elfaki Y, Herppich S, Schelmbauer C, Delacher M, Falk C, Mufazalov IA, Waisman A, Feuerer M, Huehn J. Recirculating IL-1R2$^+$ Tregs fine-tune intrathymic Treg development under inflammatory conditions. Cell Mol Immunol 2021; 18(1): 182–193
34. Cuylen S, Blaukopf C, Politi AZ, Müller-Reichert T, Neumann B, Poser I, Ellenberg J, Hyman AA, Gerlich DW. Ki-67 acts as a biological surfactant to disperse mitotic chromosomes. Nature 2016; 535(7611): 308–312
35. Zeng C, Pan F, Jones LA, Lim MM, Griffin EA, Sheline YI, Mintun MA, Holtzman DM, Mach RH. Evaluation of 5-ethynyl-2′-deoxyuridine staining as a sensitive and reliable method for studying cell proliferation in the adult nervous system. Brain Res 2010; 1319: 21–32
36. Yin L, Huang D, Liu X, Wang Y, Liu J, Liu F, Yu B. Omentin-1 effects on mesenchymal stem cells: proliferation, apoptosis, and angiogenesis *in vitro*. Stem Cell Res Ther 2017; 8(1): 224
37. Suvas S, Azkur AK, Kim BS, Kumaraguru U, Rouse BT. CD4$^+$CD25$^+$ regulatory T cells control the severity of viral immunoinflammatory lesions. J Immunol 2004; 172(7): 4123–4132
38. Shi C, Wu T, He Y, Zhang Y, Fu D. Recent advances in bone-targeted therapy. Pharmacol Ther 2020; 207: 107473
39. Tabula Muris Consortium; Overall coordination; Logistical coordination; Organ collection and processing; Library preparation and sequencing; Computational data analysis; Cell type annotation; Writing group; Supplemental text writing group; Principal investigators. Single-cell transcriptomics of 20 mouse organs creates a Tabula Muris. Nature 2018; 562(7727): 367–372
40. Li J, Wang Z, Wang J, Guo Q, Fu Y, Dai Z, Wang M, Bai Y, Liu X, Cooper PR, Wu J, He W. Amphiregulin regulates odontogenic differentiation of dental pulp stem cells by activation of mitogen-activated protein kinase and the phosphatidylinositol 3-kinase signaling pathways. Stem Cell Res Ther 2022; 13(1): 304
41. Wang T, Zhang X, Bikle DD. Osteogenic differentiation of periosteal cells during fracture healing. J Cell Physiol 2017; 232(5): 913–921
42. Yang C, Liu X, Zhao K, Zhu Y, Hu B, Zhou Y, Wang M, Wu Y, Zhang C, Xu J, Ning Y, Zou D. miRNA-21 promotes osteogenesis via the PTEN/PI3K/Akt/HIF-1α pathway and enhances bone regeneration in critical size defects. Stem Cell Res Ther 2019; 10(1): 65
43. Komori T. Functions of osteocalcin in bone, pancreas, testis, and muscle. Int J Mol Sci 2020; 21(20): 7513
44. Vimalraj S. Alkaline phosphatase: structure, expression and its function in bone mineralization. Gene 2020; 754: 144855
45. Furuta T, Miyaki S, Ishitobi H, Ogura T, Kato Y, Kamei N, Miyado K, Higashi Y, Ochi M. Mesenchymal stem cell-derived exosomes promote fracture healing in a mouse model. Stem Cells Transl Med 2016; 5(12): 1620–1630
46. Claes L, Recknagel S, Ignatius A. Fracture healing under healthy and inflammatory conditions. Nat Rev Rheumatol 2012; 8(3): 133–143
47. Nowak-Sliwinska P, Alitalo K, Allen E, Anisimov A, Aplin AC, Auerbach R, Augustin HG, Bates DO, van Beijnum JR, Bender RHF, Bergers G, Bikfalvi A, Bischoff J, Böck BC, Brooks PC, Bussolino F, Cakir B, Carmeliet P, Castranova D, Cimpean AM, Cleaver O, Coukos G, Davis GE, De Palma M, Dimberg A, Dings RPM, Djonov V, Dudley AC, Dufton NP, Fendt SM, Ferrara N, Fruttiger M, Fukumura D, Ghesquière B, Gong Y, Griffin RJ, Harris AL, Hughes CCW, Hultgren NW, Iruela-Arispe ML, Irving M, Jain RK, Kalluri R, Kalucka J, Kerbel RS, Kitajewski J, Klaassen I, Kleinmann HK, Koolwijk P, Kuczynski E, Kwak BR, Marien K, Melero-Martin JM, Munn LL, Nicosia RF, Noel A, Nurro J, Olsson AK, Petrova TV, Pietras K, Pili R, Pollard JW, Post MJ, Quax PHA, Rabinovich GA, Raica M, Randi AM, Ribatti D, Ruegg C, Schlingemann RO, Schulte-Merker S, Smith LEH, Song JW, Stacker SA, Stalin J, Stratman AN, Van de Velde M, van Hinsbergh VWM, Vermeulen PB, Waltenberger J, Weinstein BM, Xin H, Yetkin-Arik B, Yla-Herttuala S, Yoder MC, Griffioen AW. Consensus guidelines for the use and interpretation of angiogenesis assays. Angiogenesis 2018; 21(3): 425–532
48. Protopsaltis NJ, Liang W, Nudleman E, Ferrara N. Interleukin-22 promotes tumor angiogenesis. Angiogenesis 2019; 22(2): 311–323
49. Zhang L, Jiao G, Ren S, Zhang X, Li C, Wu W, Wang H, Liu H, Zhou H, Chen Y. Exosomes from bone marrow mesenchymal stem cells enhance fracture healing through the promotion of osteogenesis and angiogenesis in a rat model of nonunion. Stem Cell Res Ther 2020; 11(1): 38
50. Taylor D. Fracture and repair of bone: a multiscale problem. J Mater Sci 2007; 42(21): 8911–8918
51. Mitchell SAT, Majuta LA, Mantyh PW. New insights in understanding and treating bone fracture pain. Curr Osteoporos Rep 2018; 16(4): 325–332
52. Holmes D. Non-union bone fracture: a quicker fix. Nature 2017; 550(7677): S193
53. Marzi I. Focus on non-union of fractures. Eur J Trauma Emerg Surg 2019; 45(1): 1–2
54. Schlundt C, Bucher CH, Tsitsilonis S, Schell H, Duda GN, Schmidt-Bleek K. Clinical and research approaches to treat non-union fracture. Curr Osteoporos Rep 2018; 16(2): 155–168
55. Dülgeroglu TC, Metineren H. Evaluation of the effect of platelet-rich fibrin on long bone healing: an experimental rat model. Orthopedics 2017; 40(3): e479–e484
56. Bastian OW, Koenderman L, Alblas J, Leenen LP, Blokhuis TJ. Neutrophils contribute to fracture healing by synthesizing fibronectin$^+$ extracellular matrix rapidly after injury. Clin Immunol 2016; 164: 78–84
57. Timlin M, Toomey D, Condron C, Power C, Street J, Murray P, Bouchier-Hayes D. Fracture hematoma is a potent proinflammatory mediator of neutrophil function. J Trauma 2005; 58(6): 1223–1229
58. Ross EA, Devitt A, Johnson JR. Macrophages: the good, the bad, and the gluttony. Front Immunol 2021; 12: 708186
59. Arora S, Dev K, Agarwal B, Das P, Syed MA. Macrophages: their role, activation and polarization in pulmonary diseases. Immunobiology 2018; 223(4–5): 383–396
60. Könnecke I, Serra A, El Khassawna T, Schlundt C, Schell H, Hauser A, Ellinghaus A, Volk HD, Radbruch A, Duda GN, Schmidt-Bleek K. T and B cells participate in bone repair by infiltrating the fracture callus in a two-wave fashion. Bone 2014; 64: 155–165
61. Luo CY, Wang L, Sun C, Li DJ. Estrogen enhances the functions

of $CD4^+CD25^+Foxp3^+$ regulatory T cells that suppress osteoclast differentiation and bone resorption *in vitro*. Cell Mol Immunol 2011; 8(1): 50–58

62. Kelchtermans H, Geboes L, Mitera T, Huskens D, Leclercq G, Matthys P. Activated $CD4^+CD25^+$ regulatory T cells inhibit osteoclastogenesis and collagen-induced arthritis. Ann Rheum Dis 2009; 68(5): 744–750
63. Xu F, Guanghao C, Liang Y, Jun W, Wei W, Baorong H. Treg-promoted new bone formation through suppressing TH17 by secreting Interleukin-10 in ankylosing spondylitis. Spine 2019; 44(23): E1349–E1355
64. Wang L, Simons DL, Lu X, Tu TY, Solomon S, Wang R, Rosario A, Avalos C, Schmolze D, Yim J, Waisman J, Lee PP. Connecting blood and intratumoral T_{reg} cell activity in predicting future relapse in breast cancer. Nat Immunol 2019; 20(9): 1220–1230
65. D'Alessio FR, Tsushima K, Aggarwal NR, West EE, Willett MH, Britos MF, Pipeling MR, Brower RG, Tuder RM, McDyer JF, King LS. $CD4^+CD25^+Foxp3^+$ Tregs resolve experimental lung injury in mice and are present in humans with acute lung injury. J Clin Invest 2009; 119(10): 2898–2913
66. Mahata B, Zhang X, Kolodziejczyk AA, Proserpio V, Haim-Vilmovsky L, Taylor AE, Hebenstreit D, Dingler FA, Moignard V, Göttgens B, Arlt W, McKenzie AN, Teichmann SA. Single-cell RNA sequencing reveals T helper cells synthesizing steroids de novo to contribute to immune homeostasis. Cell Rep 2014; 7(4): 1130–1142
67. Rothem DE, Rothem L, Dahan A, Eliakim R, Soudry M. Nicotinic modulation of gene expression in osteoblast cells, MG-63. Bone 2011; 48(4): 903–909
68. Zaiss DMW, Gause WC, Osborne LC, Artis D. Emerging functions of amphiregulin in orchestrating immunity, inflammation, and tissue repair. Immunity 2015; 42(2): 216–226
69. Tamama K, Kawasaki H, Wells A. Epidermal growth factor (EGF) treatment on multipotential stromal cells (MSCs). Possible enhancement of therapeutic potential of MSC. J Biomed Biotechnol 2010; 2010: 795385